BJP British Journal of Pharmacology

DOI:10.1111/j.1476-5381.2012.02090.x
www.brjpharmacol.org

RESEARCH PAPER

Functional monoclonal antibody acts as a biased agonist by inducing internalization of metabotropic glutamate receptor 7

C Ullmer[1,*], S Zoffmann[2,*], B Bohrmann[3], H Matile[2], L Lindemann[3], PJ Flor[4] and P Malherbe[3]

[1]*DTA CV and Metabolism, Discovery Research CV & Metabolic Diseases, F. Hoffmann-La Roche AG, pRED, Pharma Research & Early Development, Basel, Switzerland,* [2]*Discovery Technologies, F. Hoffmann-La Roche AG, pRED, Pharma Research & Early Development, Basel, Switzerland,* [3]*DTA Central Nervous System, Discovery Neuroscience, F. Hoffmann-La Roche AG, pRED, Pharma Research & Early Development, Grenzacherstasse, Basel, Switzerland, and* [4]*Faculty of Biology and Preclinical Medicine, Laboratory of Molecular & Cellular Neurobiology, University of Regensburg, Regensburg, Germany*

Correspondence
Christoph Ullmer, F. Hoffmann-La Roche AG, Pharmaceuticals Division, DTA CV & Metabolic Diseases, Discovery Research CV & Metabolic Diseases, Dept. PMDM, Bldg. 70/235, Grenzacherstrasse 124, CH 4070 Basel, Switzerland. E-mail: christoph.ullmer@roche.com

*Both authors contributed equally to this work

Keywords
metabotropic glutamate receptor 7; monoclonal antibody; IgG-mediated receptor internalization; biased agonist; ERK1/2; pertussis toxin insensitive

Received
30 December 2012
Revised
18 June 2012
Accepted
25 June 2012

BACKGROUND AND PURPOSE

The $mGlu_7$ receptors are strategically located at the site of vesicle fusion where they modulate the release of the main excitatory and inhibitory neurotransmitters. Consequently, they are implicated in the underlying pathophysiology of CNS diseases such as epilepsy and stress-related psychiatric disorders. Here, we characterized a selective, potent and functional anti-$mGlu_7$ monoclonal antibody, MAB1/28, that triggers receptor internalization.

EXPERIMENTAL APPROACH

MAB1/28's activity was investigated using Western blot and direct immunofluorescence on live cells, *in vitro* pharmacology by functional cAMP and [^{35}S]-GTPγ binding assays, the kinetics of IgG-induced internalization by image analysis, and the activation of the ERK1/2 by ELISA.

KEY RESULTS

$mGlu_7$/$mGlu_6$ chimeric studies located the MAB1/28 binding site at the extracellular amino-terminus of $mGlu_7$. MAB1/28 potently antagonized both orthosteric and allosteric agonist-induced inhibition of cAMP accumulation. The potency of the antagonistic actions was similar to the potency in triggering receptor internalization. The internalization mechanism occurred via a pertussis toxin-insensitive pathway and did not require $G\alpha_i$ protein activation. MAB1/28 activated ERK1/2 with potency similar to that for receptor internalization. The requirement of a bivalent receptor binding mode for receptor internalizations suggests that MAB1/28 modulates $mGlu_7$ dimers.

CONCLUSIONS AND IMPLICATIONS

We obtained evidence for an allosteric-biased agonist activity triggered by MAB1/28, which activates a novel IgG-mediated GPCR internalization pathway that is not utilized by small molecule, orthosteric or allosteric agonists. Thus, MAB1/28 provides an invaluable biological tool for probing $mGlu_7$ function and selective activation of its intracellular trafficking.

Abbreviations

7TMD, seven-transmembrane domain; AMN082, N,N'-dibenzhydrylethane-1,2-diamine dihydrochloride; ARF6, ADP-ribosylation factor 6; CaM, calmodulin; L-AP4, L-2-amino-4-phosphonobutyrate; mGlu receptor, metabotropic glutamate receptor; PMA, phorbol 12-myristate 13-acetate; PTX, pertussis toxin; RT, room temperature

Introduction

GPCRs constitute a family of cell surface proteins capable of activation through a wide diversity of extracellular signals such as hormones, neurotransmitters, ions, growth and development factors (Foord *et al.*, 2005). These heptahelical receptors transduce and amplify cellular signals through various mechanisms, primarily by the activation of heterotrimeric G proteins, which leads to canonical second messenger signalling and by β-arrestin functions upon phosphorylation of the activated GPCR by G-protein coupled receptor kinases. The latter induces receptor internalization and sequestration from G proteins and can stimulate other signals, mainly intracellular kinase activities (DeWire *et al.*, 2007). The discovery of biased agonists showed that the G-protein and β-arrestin coupled functions could be triggered independently (Gesty-Palmer *et al.*, 2006; Drake *et al.*, 2008).

Based on protein sequence similarity, phylogenetic analyses revealed the existence of three major receptor classes (Foord *et al.*, 2005). Members from class C are activated by extracellular calcium, pheromones, GABA and L-glutamate which bind within a common large N-terminal extracellular domain composed of a cysteine-rich domain and a Venus Flytrap module (Pin *et al.*, 2003). In contrast to class A GPCRs, in which the agonist-binding site is frequently located within the seven-transmembrane domain (7TMD), the 7TMD region of class C receptors form a binding pocket for ligands acting as positive or negative allosteric modulators (Pin *et al.*, 2004). Metabotropic glutamate receptors (mGlu receptors) are members of class C and are activated by the major excitatory neurotransmitter of the mammalian brain, L-glutamate, and act as important pre- and postsynaptic regulators of neurotransmission in the CNS. The eight mGlu receptors can be divided into three groups based on sequence similarity, signal transduction mechanisms and pharmacology. Group I consists of mGlu$_1$ and mGlu$_5$ receptors that activate phospholipase C. Both group II (mGlu$_2$ and mGlu$_3$) and group III (mGlu$_4$, mGlu$_6$, mGlu$_7$ and mGlu$_8$) receptors [nomenclature follows Alexander *et al.* (2011)] inhibit adenylate cyclase when expressed in heterologous expression systems but differ in their ligand recognition selectivity and G protein coupling specificity (Conn and Pin, 1997). The crystal structures of the extracellular ligand-binding region showed that the mGlu receptors exist as homodimers linked by a disulfide bridge at the hinge region between the 7TMD and the large N-terminal extracellular domain (Kunishima *et al.*, 2000). Of all group III mGlu receptors, mGlu$_7$, the focus of the work presented here, is the most widely distributed presynaptic (as auto- and hetero-receptors) and also postsynaptic receptor in the brain (Kinoshita *et al.*, 1998; Kosinski *et al.*, 1999). It is expressed in regions that are known to be critical for the manifestation of anxiolytic and antidepressant action, such as the lateral septal nucleus, frontal cortex, amygdala, hippocampus and the locus coeruleus (Kinoshita *et al.*, 1998). Like most other group III mGlu receptors, mGlu$_7$ is thought to provide mainly negative feedback, limiting transmitter release at synapses in a frequency-dependent fashion (Cartmell and Schoepp, 2000). These synapses may in fact include non-glutamatergic synapses such as GABAergic terminals of interneurons (Somogyi *et al.*, 2003). In the past, the pharmacology of mGlu$_7$ could only be explored using L-2-amino-4-phosphonobutyrate (L-AP4), which is a presynaptic inhibitor of neurotransmitter release and a non-selective orthosteric agonist for all group III mGlu receptor subtypes (Schoepp *et al.*, 1999). Recently, a brain penetrant, subtype-selective agonist, AMN082 (Mitsukawa *et al.*, 2005), has been identified that activates mGlu$_7$ receptor signalling via an allosteric site in the transmembrane domain. Despite the different binding sites, both agonists stimulate Gα_i-coupled inhibition of cAMP accumulation.

The intracellular C-terminal tail of mGlu$_7$ has many interesting features that play an important role in mGlu$_7$ signal transduction. It has been reported that binding of calmodulin (CaM) to the Ca^{2+}/CaM-binding region of the mGlu7 C-tail promotes G protein-mediated signalling by displacing G protein βγ subunits from the C-terminal tail (O'Connor *et al.*, 1999). Structural studies indicate that Ca^{2+}/CaM binding to mGlu$_{7a}$ includes interactions with both Ser^{862}, a target site for phosphorylation by protein kinase C (Nakajima *et al.*, 1999; Dev *et al.*, 2000; Airas *et al.*, 2001), and the G βγ recognition motif (El Far *et al.*, 2001). Recent structural studies have also identified the region from amino acids 856–879 of mGlu$_7$ C-tail to be responsible for CaM binding (Scheschonka *et al.*, 2008). Moreover, the C-tail of mGlu$_{7a}$ displays a PDZ-binding motif (LVI) that has been shown to interact with PICK1 (protein interacting with C kinase 1) (El Far *et al.*, 2000), and this interaction is involved in synaptic transmission and plasticity (Perroy *et al.*, 2002). Moreover, mGlu$_7$ has been implicated in the pathophysiology of numerous CNS disorders such as epilepsy and stress-related psychiatric disorders (Niswender *et al.*, 2005). Investigations with knockout (KO) mice and siRNA knockdown indicate that mGlu$_7$ plays a role in anxiety, extinction of fear and aversion learning, spatial memory and hormonal response to stress (Masugi *et al.*, 1999; Cryan *et al.*, 2003; Mitsukawa *et al.*, 2006). Also, mGlu$_7$ facilitates extinction of aversive memories and controls amygdala plasticity (Fendt *et al.*, 2008). The discovery of AMN082 has provided an invaluable tool to explore the potential of mGlu$_7$ as a therapeutic target. Paradoxically, AMN082 displayed an antidepressant-like behaviour in mice (Palucha *et al.*, 2007), which was similar to that observed in mGlu$_7$ KO mice (Cryan *et al.*, 2003). Furthermore, the antidepressant-like action induced by AMN082 was shown to be mediated through the 5-hydroxytryptaminergic system (Palucha-Poniewiera *et al.*, 2010). Administration of AMN082 has also been shown to promote the proliferation of neural progenitor cells via MAPK signalling pathways (Tian *et al.*, 2010). Nevertheless, a recent report profiling AMN082 in rat liver microsomes has revealed a rapid metabolism ($t_{1/2}$ < 1 min) to a major metabolite, N-benzhydrylethane-1,2-diamine (Met-1). Interestingly, Met-1 had appreciable affinity as a serotonin transporter inhibitor and produced *in vivo* antidepressant-like activity upon acute administration. Consequently, the reported *in vivo* actions of AMN082 might involve mechanisms other than those mediated by mGlu$_7$ (Sukoff Rizzo *et al.*, 2011).

Given the diverse functioning of mGlu$_7$ receptors and a lack of selective *in vivo* active ligands, the development of novel selective tools is crucial for understanding the physiological and pathophysiological role of these receptors. In the current study, we characterized a functional monoclonal antibody, MAB1/28, that potently and specifically binds the native N-terminal domains of dimeric mGlu$_7$ receptors. We

demonstrated that MAB1/28 act as an allosteric biased agonist of the $mGlu_7$, which potently antagonizes both orthosteric and allosteric agonists via clearance of $mGlu_7$ from plasma membranes, and by itself triggers the G protein-independent internalization pathway involving activation of MAPK/ERK signalling. Analysis of recent publications suggests that this mechanism might be applicable to GPCR receptor families other than class C.

Methods

Materials

AMN082 was synthesized at F. Hoffmann-La Roche Ltd. LY341495 ((2*S*)-2-amino-2-[(1*S*,2*S*)-2-carboxycyclopprop-1-yl]-3-(xanth-9-yl) propanoic acid) and L-AP4 were purchased from Tocris Bioscience (Bristol, UK). Krebs Ringer, forskolin, IBMX, pertussis toxin (PTX), Hoechst 33258, phorbol 12-myristate 13-acetate (PMA) and fatty acid-free BSA were obtained from Sigma (Buchs, Switzerland). [^{35}S]- GTPγ, SPA beads (WGA), ECL Plus detection Kit and peroxidase (POD)-labelled goat anti-mouse or anti-rabbit IgG antibody were purchased from GE Healthcare (Chalfont St. Giles, UK). FITC-rabbit anti-mouse IgG (H + L), rabbit anti-mouse IgG (H + L) specific antibody, Alexa Fluor 532 goat anti-mouse IgG (H + L), Alexa Fluor 647 goat anti-mouse IgG (H + L) and Alexa Fluor 647 goat anti-rabbit IgG were purchased from Invitrogen (Carlsbad, CA, USA) and the anti-$mGlu_6$ rabbit polyclonal antibody ab90866 was purchased from Abcam (Cambridge, UK). TrueBlue Chloride and Hoechst 33852 were obtained from Molecular Probes (Eugene, OR, USA).

mGlu$_7$ receptor expression in mammalian cells

Rat $mGlu_{7a}$ receptor cDNA (GenBank: D16817) was inserted into pcDNA3.1 (Invitrogen). CHO cells deficient in dihydrofolate reductase activity (CHO-dhfr$^-$) harbouring a luciferase reporter gene under the control of 5 cAMP-responsive elements (CHO-DUKX-CRE-luci cells) were grown to 80% confluency in growth medium [DMEM supplemented with 1× HT, 10% dialysed fetal calf serum (FCS), 100 μg·mL^{-1} penicillin and 100 μg·mL^{-1} streptomycin] and were transfected with pcDNA3.1- $mGlu_{7a}$ using Lipofectamine plus (Invitrogen) according to the manufacturer's instructions. Clones were isolated in limited dilution conditions and identified by activities in the reporter gene assay. Cells were stimulated with 1 μmol·L^{-1} forskolin and 0.5 mmol·L^{-1} L-AP4 in the assay buffer (5 mmol·L^{-1} KCL, 154 mmol·L^{-1} NaCl, 2.3 mmol·L^{-1} CaCl2, 5 mmol·L^{-1} NaHCO3, 1 mmol·L^{-1} MgCl2, 5.5 mmol·L^{-1} glucose, 5 mmol·L^{-1} HEPES, 10 μmol·L^{-1} IBMX, pH 7.4). After 4 h the supernatant was exchanged with lysis buffer (25 mmol·L^{-1} Tris, 0.4 mmol·L^{-1} DTT, 0.4 mmol·L^{-1} EDTA, 0.2% glycerol, 0.2% Triton X-100, pH 7.8) and the luciferase activity measured. Responses ranged from 0% to about 83% depression. A stable, clonal cell line (CHO-DUKX-CRE-luci-$rmGlu_{7a}$, clone 83) displaying the greatest inhibition of forskolin-mediated luciferase activity was identified as giving consistently good responses for up to at least 20 passages.

Animals

Immunization was conducted with female BALB/c mice (NMRI,Charles River Laboratories, Sulzfeld, Germany) maintained on a standard diet. Mice were housed individually at approximately 21°C and 55–65% relative humidity, and a 12 h light/dark cycle was maintained. After delivery, animals were acclimatized to the facility for 6–7 days before experimental procedures were initiated. All experiments were conducted under authorization from the Swiss Federal Veterinary Office and the Association for Assessment and Accreditation of Laboratory Animal Care International. All studies involving animals are reported in accordance with the ARRIVE guidelines (Kilkenny *et al.*, 2010; McGrath *et al.*, 2010).

Production of MABs

For whole cell immunization, CHO-DUKX-CRE-luci-$rmGlu_{7a}$ cells were transiently transfected with the expression plasmid for $rmGlu_7$ using Lipofectamine plus and frozen in liquid nitrogen for immunizations. Five mice were immunized by repeated i.v. injection of living cells. Animals were tail bled after the several boosts, and sera were tested to select the best candidate for fusion. From the animals showing a specific immune response to $mGlu_7$ receptors, the spleens were removed and the cells were fused to Ag8 cells according to Kohler and Milstein (1975). Positive hybridomas were selected by immunofluorescence on CHO-DUKX-CRE-luci-mGlu7 transfected cells. Clonal purity was achieved in limited dilution conditions.

Membrane preparation

CHO-DUKX-CRE-luci-$rmGlu_{7a}$ cells were cultured and harvested when they reached 80–95% confluency, followed by homogenization in 20 mmol·L^{-1} HEPES, 10 mmol·L^{-1} EDTA, pH 7.4 using a Polytron and centrifugation at 47 800× *g* at 4°C for 30 min. The pellet was then rehomogenized twice in 20 mmol·L^{-1} HEPES, 0.1 mmol·L^{-1} EDTA, pH 7.4, and centrifuged (47 800× *g*, 4°C, 30 min). The final pellet was then resuspended in the same buffer at a protein concentration of 2–3 mg·mL^{-1}, aliquoted, frozen on dry ice and stored at –70°C.

Membrane-based ELISA of transfected CHO cells

The cell membranes were diluted in PBS, transferred to wells of an ELISA plate (Nunc MaxiSorp 96-well ELISA plates) and incubated overnight at 4°C. Immobilized membranes were blocked with 1% BSA, and then tested with antibodies in hybridoma supernatants. A horseradish POD-labelled anti-mouse IgG (RAM-HRPO; Nordic, Tillburg, The Netherlands) was used as the secondary antibody, and binding was detected colorimetrically by reaction with tetramethylbenzidine.

Immunocytochemistry and time-lapse microscopy

Twenty-four hours after transfection, the CHO-dhfr$^-$ cells were transferred to poly-D-lysine-coated coverslips in growth medium. Coverslips were placed on ice, IgG (MAB1/28) or IgG-Alexa488 (Alexa488 fluorophore conjugated MAB1/28) added (1:100) and incubated for 30 min in DMEM, washed

twice with DMEM before the addition of a rabbit anti-mouse FITC antibody (1:100), incubated 30 min still on ice, and after two wash steps as before mounted with glycerol/PBS (1:1).

CHO-DUKX-CRE-luci-rmGlu$_{7a}$ cells were plated on a Lab-TEK™ Chamber Slide in growth medium. The chamber slide was placed on ice, medium was gently removed and IgG-Alexa488 fluorophore conjugated MAB1/28 (1:20) added in medium without additives. After incubation for 1 h, cells were washed twice with ice-cold medium and the chamber slide containing fresh ice-cold medium was mounted on the microscope table maintained in a humidified atmosphere with 5% CO_2 at 37°C. Time-lapse microscopy was performed using Leica TCS SP2 AOBS confocal laser scanning microscope equipped with a Ludin incubation chamber system for life cell imaging (Life Imaging Services, Basel, Switzerland). Confocal images were collected with a spacing of 1 µm in the *z*-axis using a HCX PL APO 63.0.x 1.2 IMM BD UV objective and visualized with Imaris software (Bitplane, Zürich, Switzerland).

Western blot

For Western blot analysis, samples containing 0.5 µg of membrane proteins from CHO-DUKX-CRE-luci-rmGlu$_{7a}$ or CHO-DUKX-CRE-luci control cells were prepared under reducing and non-reducing conditions. Proteins were separated by 4–12% Nupage gel (Invitrogen) and electroblotted onto a nitrocellulose membrane. After blocking, the blot was incubated with mouse monoclonal antibody, MAB1/28 (5 µg·mL^{-1}) or a commercially available anti-mGlu$_7$ rabbit polyclonal antibody (Upstate/Millipore, Billerica, MA, USA; at 1:10 000 dilution). A POD-labelled goat anti-mouse or anti-rabbit IgG antibody (at dilution 1:10 000) was used as a secondary antibody. The signal was revealed using the ECL Plus detection Kit.

[^{35}S]-GTPγ binding assay

Membrane fractions were washed and diluted in assay buffer (20 mmol·L^{-1} HEPES, 10 mmol·L^{-1} $MgCl_2$, 100 mmol·L^{-1} NaCl, 2 mmol·L^{-1} EGTA, 10 µmol·L^{-1} GDP, pH 8.0), homogenized briefly using a Polytron and incubated for 10 min at 30°C. Following pre-incubation, assay mixtures were prepared in 96-well microtitre plates. The composition of the assay mixtures in a final volume of 200 µL per well was as follows: 20 mmol·L^{-1} HEPES, 10 mmol·L^{-1} $MgCl_2$, 100 mmol·L^{-1} NaCl, 2 mmol·L^{-1} EGTA, 10 µmol·L^{-1} GDP, pH 8.0, 10 µg membrane protein (pretreated as described above), 1.5 mg wheat germ agglutinin SPA beads, 0.05–0.2 nmol·L^{-1} [^{35}S]-GTPγ and the test compounds (agonists and/or antibody) at the appropriate concentrations. Non-specific binding was measured in the presence of unlabelled S-GTPγ in excess (10 µmol·L^{-1}). The samples were incubated at room temperature (RT) for 3 h (with shaking) before the SPA beads were sedimented by centrifugation at 200× *g* for 10 min at RT. The plates were then counted in a Packard TopCount (Canberra Packard S.A., Zürich, Switzerland).

Immunohistochemistry in rodent brain sections

mGlu$_7^{-/-}$ mice were generated as described previously (Sansig *et al.*, 2001) from E14 (129/Ola) embryonic stem cells. mGlu$_7^{-/-}$ and mGlu$_7^{+/+}$ littermates used here carried wild-type or mutant mGlu$_7$ alleles on a 14th-generation (F14) C57BL/6 genetic background. Cryosections of 2-month-old Wistar rat, 6-month-old C57Bl/6J, age-matched mGlu$_7^{-/-}$ and mGlu$_7^{+/+}$ mouse brains were prepared at 10 µm nominal thickness, dipped in ice-cold acetone for 2 min and washed in PBS. Non-specific binding sites were blocked using Ultra V block (LabVision, Fremont, CA, USA) for 5 min followed by a PBS wash and incubation in power block solution (BioGenex, San Ramon, CA, USA) with 10% normal sheep serum for 20 min. MAB1/28 was used at 10 µg·mL^{-1} in PBS with power block solution and 10% normal sheep serum for 1 h at RT. After washing, MAB1/28 was detected by secondary goat anti-mouse IgG conjugated with AlexaFluor555 (Molecular Probes). Images were recorded with a GenePix Personal 4100A microarray scanner and a Leica SP2 confocal microscope (Leica Microsystems, Wetzlar, Germany).

cAMP assay

cAMP was measured using cAMP-Nano-TRF detection kit (Roche Diagnostics, Penzberg, Germany). CHO-DUKX-CRE-luci-rmGlu$_{7a}$ cells were seeded 17–24 h prior to the experiment 50 000 cells per well in a black 96-well plate with flat clear bottom (Corning, Wiesbaden, Germany) in growth medium with 7.5% dialysed FCS and incubated in 5% CO_2 at 37°C in a humidified incubator. The growth medium was exchanged with Krebs Ringer bicarbonate buffer with 1 mmol·L^{-1} IBMX and incubated at 30°C for 30 min. Antagonist or antibody was added for 15 min before the addition of 0.3 mmol·L^{-1} L-AP4 and 3 µmol·L^{-1} forskolin to a final assay volume of 100 µL and incubated for 30 min at 30°C. The assay was stopped by the addition of 50 µL lysis reagent (Tris, NaCl, 1.5% Triton X100, 2.5% NP40, 10% NaN3) and 50 µL detection solutions (20 µmol·L^{-1} mAb Alexa700-cAMP 1:1 and 48 µmol·L^{-1} Ruthenium-2-AHA-cAMP) and shaken for 2 h at RT. The time-resolved energy transfer was measured using a TRF reader (Evotec Technologies GmbH, Hamburg, Germany), equipped with a ND:YAG laser as excitation source. The plate was measured twice with the excitation at 355 nm and at the emission with a delay of 100 ns and a gate of 100 ns, total exposure time 10 s at 730 (bandwidth 30 nm) or 645 nm (bandwidth 75 nm), respectively. The measured signal at 730 nm had to be corrected for the ruthenium background, the direct excitation of Alexa and the buffer control. The FRET signal was calculated as follows: FRET = T730-Alexa730-P(T645-B645) with P = Ru730-B730/Ru645-B645, where T730 was the test well measured at 730 nm or T645 at 645 nm, B730 and B645 were the buffer controls at 730 and 645 nm respectively. cAMP content was determined from the function of a standard curve spanning from 10 µmol·L^{-1} to 0.13 nmol·L^{-1} cAMP.

Quantification of membrane to cytoplasm translocation of mGlu$_7$

CHO-DUKX-CRE-luci-rmGlu$_{7a}$ cells were plated (at 25 000 cells per well in 100 µL growth medium) in a 96-well special optics plate (Corning). The cells were incubated at 37°C in a humidified cell culture incubator with 5% CO_2 to allow the cells to adhere. On the day of the experiment (24 h after plating), the growth medium was gently aspirated and 100 µL

per well of 3 μmol·L^{-1} Hoechst 33258 and 2 μg·mL^{-1} TrueBlue Chloride solution (prepared with 37°C warm buffer-I: 1 × HBSS, 20 mmol·L^{-1} HEPES, 0.1% BSA) was added and the plate incubated for 30 min at 37°C in a humidified incubator. The cells were washed once with 100 μL per well of buffer-I at 37°C.

Cell membrane mGlu$_7$ staining – Prewarmed MAB1/28 or Fab1 solution (60 μL per well) was added and the plate was incubated for 30 min at 37°C. The cells were quickly washed three times with 100 μL of PBS at RT. The plate was transferred to an ice bath, 60 μL per well of the ice-cold Alexa532 goat anti-mouse secondary antibody solution (Invitrogen, 2.5 μg·ml^{-1} in PBS) was added and the plate was incubated for 60 min. The cells were washed three times with 100 μL per well ice-cold PBS; 150 μL per well of chilled methanol (–20°C) was added and the plate incubated on ice for 10 min. The wells were washed with 100 μL per well of PBS at RT, 100 μL per well of 4% formaldehyde in PBS was added and the plate was incubated for 15 min at RT. The wells were washed once with PBS at RT.

Cytoplasmic mGlu$_7$ staining

The cell membranes were permeabilized by incubation with a 0.25% Triton X-100 solution in PBS at RT for 5 min. The cells were washed once with PBS and incubated with a 10% solution of goat serum diluted in PBS for 30 min. The goat serum was replaced with a freshly prepared 1:400 solution of Alexa647 goat anti-mouse secondary antibody diluted in PBS. The cells were incubated at RT for 30 min, washed three times with 100 μL per well of PBS at RT. Then 100 μL per well of 4% formaldehyde was added, and the plates were incubated for 15 min at RT. The solution was replaced with 150 μL PBS per well.

Quantification of mGlu$_7$ internalization

Internalization of antibody (MAB1/28 or Fab1 fragments) was quantified using an Opera QEHS high content screening (HCS) plate reader (Evotec Technologies). This is equipped with an inverted confocal fluorescence microscope with automatic image acquisition. Acapella, the image analysis software integrated in the reader, is programmed to localize and determine the fluorescent intensity of pre-defined objects. The analysis was based on three images acquired simultaneously of samples stained with a DNA-specific fluorophore (Hoechst 33258), the homogeneous intact cell stain TrueBlue and the two secondary antibodies with different conjugated fluorophores (Alexa532-cell membrane mGlu$_7$ and Alexa647-intracellular mGlu$_7$). The DNA and TrueBlue stains permitted the determination of the number, position, size and shape of the nuclei and the outline of the cytoplasm to be determined respectively. The Alexa532- and Alexa647-labelled secondary antibody staining permitted cell membrane and cytoplasmic mGlu$_7$ to be measured respectively. EC_{50} values were determined using the software GraphPad Prism (GraphPad Software, San Diego, CA), applying a non-linear regression of the equation {y = Bottom + (Top – Bottom)/(1 + 10[(logEC_{50}-x)* nH)]}.

Kinetics of IgG internalization

The experiment was carried out as above, with the following modifications. The cells were incubated with primary antibody or Fab fragments at 37°C for up to 1 h, then transferred to ice and the solutions replaced with fresh ice-cold solutions of primary antibody or Fab fragments for 1 h before staining with secondary antibodies. After the last staining, the cells were fixed in formaldehyde (15 min, RT) before incubation with Hoechst 33258 and TrueBlue in PBS followed by a second fixation in 4% formaldehyde for 15 min at RT.

Construction of chimeric receptors

cDNAs encoding chimeric rmGlu$_6$ and rmGlu$_7$ receptors were constructed using crossover PCR. The rmGlu$_6$/mGlu$_7$ receptor construct contains 565 aa derived from the N-terminal extracellular region of the rat mGlu$_6$ and the remaining C-terminal portion of the rat mGlu$_{7a}$ receptor, comprising the entire transmembrane region; the rmGlu$_7$/mGlu$_6$ construct is essentially the reverse chimera with the fusion point at amino acid 576.

Expression of additional mGlu receptor constructs in mammalian cells

Cell culture was essentially performed as described in Lindemann *et al*. (2011). For immunohistochemistry, HEK-293 and CHO cells were transiently transfected with the following cDNAs (GenBank accession numbers and vectors in brackets): human mGlu$_4$ (NM_000841; pCDNA3.1(-)), rat mGlu$_6$ (NM_022920.1; pCDNA3.1(-)), rmGlu$_6$/mGlu$_7$ and rmGlu$_7$/mGlu$_6$ (pcDNA3.1). The transfections were performed with Lipofectamine (Invitrogen) according to the manufacturer in wild-type cells seeded 24 h before in 75 cm^2 cell culture flasks (Nunc, Roskilde, Denmark) at approximately 50% confluence, using 8.6 μg of plasmid encoding each receptor construct mixed with 1.7 μg pEGFP-N1 (Clontech, Mountain View, CA, USA) per flask. Furthermore, HEK-293 cell lines stably expressing human mGlu$_{1a}$ (NM_000838; pcDNA5/FRT/TO), human mGlu$_2$ (NM_000839; pcDNA5/FRT/TO), human mGlu$_3$ (NM_000840; pcDNA5/FRT/TO), human mGlu$_{5a}$ (D28538; pcDNA5/FRT/TO) and human mGlu$_8$ (NM_000845.2; pcDNA5/FRT/TO) were used; the cell lines stably expressing mGlu$_2$ and mGlu$_8$ also stably expressed the chimeric G protein Gα16 (mGlu$_2$) or Gα15 (mGlu$_8$).

Cell culture for selectivity of antibody immunohistochemistry towards other mGlu receptors

Cells expressing mGlu$_{1-8}$ as described above, either stably or 24 h after transfection, were detached with trypsin and seeded in a 96-well black/clear bottom plates (BD-Falcon 323519; Beckton-Dickinson, Franklin Lakes, NJ, USA) in parallel to wild-type HEK-293 and CHO cells at a seeding density of 12 000 and 20 000 cells per well (HEK293) and 7000 and 10 000 per well (CHO), respectively, in 100 μL growth medium per well.

Immunohistochemistry

Immunohistochemistry and quantification of immunostain with 68 nmol·L^{-1} of the antibody 1/28 were carried out as described for mGlu$_7$ above for detection of membrane-bound immunostain, with the modification that a fixation step was

introduced after the primary staining and the following secondary stain was carried out at RT.

Epitope mapping with mGlu$_{6/7}$ chimeric constructs

Transiently transfected HEK cells harvested 24 h after transfection, CHO-DUKX-CRE-luci-rmGlu$_{7a}$ cells and HEK wild-type cells were seeded in 96-well black/clear bottom plates (BD-Falcon plates) in 100 µL growth medium per well.

Immunocytochemistry with MAB1/28 was carried out after 48 h, using a protocol modified from the approach described for mGlu$_7$. Briefly, after Hoechst and TrueBlue staining, the cells were fixed with 4% formaldehyde in PBS and permeabilized before immunostain with primary antibody (68 nmol·L^{-1} 1/28 and mGlu$_6$ polyclonal antibody) and secondary antibody labelled with Alexa Fluor 647 (goat anti-mouse and donkey anti-rabbit respectively). Transfection efficiency was at least 20% as estimated by co-transfection with an eGFP expressing plasmid. Expression of mGlu$_6$ and chimeric mGlu$_7$/mGlu$_6$ was confirmed by immunostaining with anti-mGlu$_6$ rabbit polyclonal antibody.

Ca^{2+} mobilization assay

The potency of MAB1/28 was tested for agonist and antagonist activity on hmGlu$_1$, hmGlu$_2$, hmGlu$_5$ and hmGlu$_8$ in parallel with reference agonists and antagonists. For those receptors on which an activity of the antibody was detected, the Fab1 fragment was also tested. Cells expressing the target receptors in combination with chimeric G proteins (mGlu$_2$, mGlu$_8$) were seeded at 5×10^4 cells per well in poly-D-lysine-coated, 96-well, black/clear-bottomed plates. After 24 h, the cells were loaded for 1 h at 37°C with 2.5 µmol·L^{-1} Fluo-4 acetoxymethyl ester in loading buffer (1 × Hank's balanced salt solution and 20 mmol·L^{-1} HEPES). The cells were washed five times with loading buffer to remove excess dye, and intracellular calcium mobilization (intracellular calcium concentration) was measured using an FDSS7000 device (Hamamatsu, Solothurn, Switzerland).

For the measure of agonist activities, the antibody MAB1/28, Fab1 fragments (mGlu$_8$) and reference compounds (mGlu$_1$, mGlu$_5$: L-glutamate, qusiqualate; mGlu$_2$: L-glutamate, LY354740; mGlu$_8$: L-AP4) were added to the cells in serial dilutions while fluorescence was recorded for 5 min. For measuring antagonist activities, the antibody, Fab1 fragments (mGlu$_8$) and serial dilutions of reference compounds (mGlu$_1$: CPCCOEt; mGlu$_2$: LY341495; mGlu$_5$: MPEP; mGlu$_8$: MSOP) were added to the cells. After incubation for 5 min at 37°C, agonists (mGlu$_1$, mGlu$_2$, mGlu$_5$: L-glutamate; mGlu$_8$: L-AP4) were added at a concentration triggering 60–80% of the maximal response which was determined daily in a separate experiment. Responses were measured as peak increase in fluorescence recorded after the addition of test compounds and reference agonists (testing for agonist activity), or after the addition of agonists following the pre-incubation of cells with the test compounds (testing for antagonist activity), minus baseline fluorescence (i.e. fluorescence without addition of agonist). Data are expressed as % control relative to baseline fluorescence (agonist activity) or relative to the maximal stimulant effect induced by a saturating concentration of the agonist measured on the same plate. Inhibition curves were fitted using XLfit software (ID Business Solutions, Guildford, UK) according to the Hill equation $y = 100/(1 + (x/IC_{50})n_H)$, where n_H is the slope factor.

IgG-induced p44/42 MAPK activities

Cells stably expressing the mGlu$_7$ receptor were seeded in growth medium in 6-well plates. The next day, medium was replaced with 2 mL starvation medium (Opti-MEM with 0.1% fatty acid-free BSA). The following day cells were stimulated with compound in 150 µL starvation medium for the indicated times at 37°C, otherwise cells were stimulated for 5 min. Cells were washed with ice-cold PBS and lysed in 150 µL buffer containing 1 mmol·L^{-1} β-glycerophosphate, 1 mmol·L^{-1} EDTA, 1 mmol·L^{-1} EGTA, 1 µg·mL^{-1} leupeptin, 150 mmol·L^{-1} sodium chloride, 2.5 mmol·L^{-1} sodium phosphate, 20 mmol·L^{-1} Tris-CI, 1 mmol·L^{-1} PMSF and 1% Triton X-100, scraped off and sonicated on ice. After centrifugation, the supernatant was analysed for the product of p44/42 MAPK activity using the PathScan™ Sandwich ELISA kit (Cell Signalling, Beverly, MA, USA) according to the manufacturer's instructions. Absorbance (450 nm) was read using the EnVision reader (Perkin Elmer, Waltham, MA, USA).

Results

Generation and epitope mapping of anti-mGlu$_7$ MABs

To generate an anti-mGlu$_7$ antibody that recognizes only extracellular epitopes of the receptor, intact CHO cells expressing functional rmGlu$_7$ *in vitro* were used to immunize mice. After several boostings, positive antisera were obtained and spleen cells were fused with myeloma cells for cloning. The resulting hybridoma clones were screened by ELISA and immunofluorescence (IF) assays. Several hybridoma clones showed strong immunoactivities in the ELISA analyses only with membranes from CHO rmGlu$_7$ expressing cells (Figure 1A), but not with CHO non-transfected control cells (Figure 1B). The hybridoma clones exhibited similar ELISA results when CHO cells expressing human mGlu$_7$ were used (data not shown). IgG classification of hybridoma clones showed that the mouse MABs belong to IgG2 subclass (Figure 1C). Furthermore, five MABs exhibited a strong IF signal on CHO cells expressing rat or human mGlu$_7$, indicating that the MABs bind to mGlu$_7$ on the cell surface. However, these MABs did not produce any IF signal on CHO cells that had been mock-transfected with a plasmid expressing GPR40 protein used as a negative control (Figure 1C). CHO cells expressing rmGlu$_{7a}$ displayed a strong cell surface IF after staining with MAB1/28 (Figure 1D) while no IF staining was seen with MAB1/28 on CHO cells expressing rmGlu$_2$ (Figure 1E). The observed cell surface staining by MAB1/28 therefore appeared to be specific and selective for mGlu$_7$. To evaluate further the selectivity of MAB1/28 immunostaining, live cells expressing the mGlu receptors 1–8 were stained with the primary antibody MAB1/28. After fixation, the immunostain was visualized with Alexa Fluor 647 conjugated secondary antibody. The staining intensity at the cell membrane region is shown in Figure 1F. MAB1/28 immunostaining was only detected on the membrane of mGlu$_7$ expressing cells.

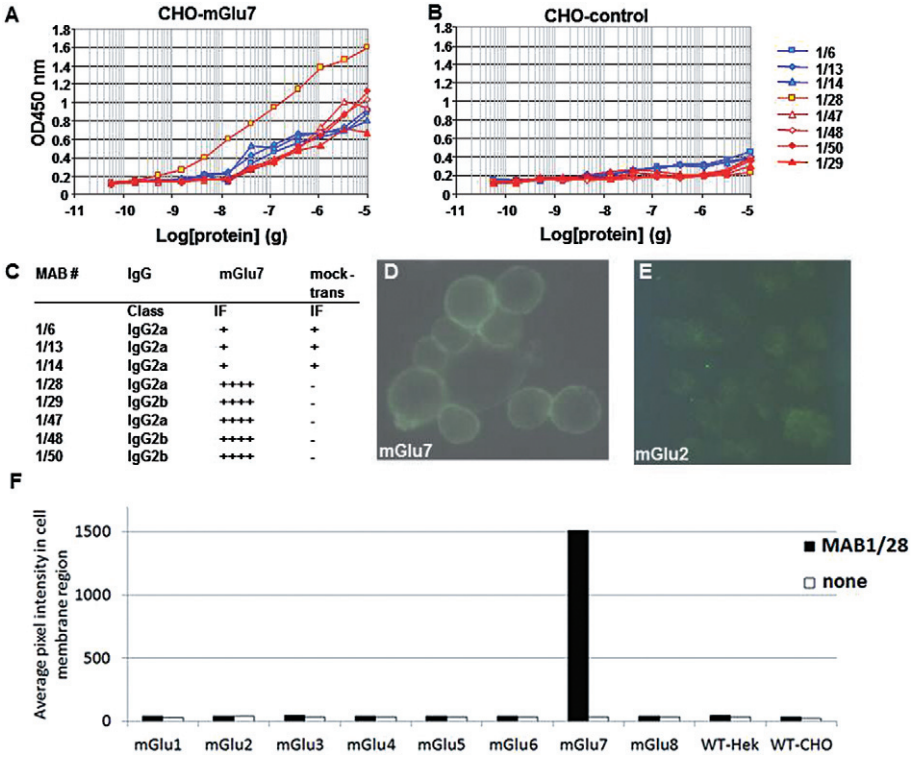

Figure 1

Characterization of $mGlu_7$ MABs. ELISA analyses of MABs using membrane preparations from CHO-DUKX-CRE-luci-$rmGlu_{7a}$ stable cell line 83 (A) and non-transfected CHO-DUKX-CRE-luci control cells (B). IgG classification and immunofluorescence analyses of MABs using CHO $mGlu_7$ expressing cells or the CHO cells mock transfected with plasmid (expressing GPR40 protein) as a negative control, and FITC-rabbit anti-mouse IgG as secondary antibody are summarized in (C). IF on live CHO-DUKX-CRE-luci-$rmGlu_{7a}$ cell line 83 (D) and CHO-DUKX-CRE-luci-$rmGlu_2$ cell line 17, which was used as a negative control for selectivity (E) by MAB1/28 using FITC-rabbit anti-mouse IgG as secondary antibody. (F) Live cells expressing the mGlu receptors 1–8 were stained with the primary antibody MAB1/28. After fixation, the immunostain was visualized with Alexa647-conjugated secondary antibody. The staining intensity at the cell membrane region was identified using high content analysis and the average immunostain pixel intensity calculated. The bars show average immunostain intensity for the cell population. The data are representative of two independent experiments.

The MABs were further characterized in the cAMP functional assay. Forskolin (3 $\mu mol \cdot L^{-1}$) stimulated adenylate cyclase to 100% and the $mGlu_7$ agonist L-AP4 inhibited this activity to 30% in the CHO cells expressing $mGlu_7$. MAB 1/14, which was negative in the IF assay, had no effect on the inhibition by L-AP4 of forskolin-stimulated cAMP accumulation (Figure 2A), whereas MAB1/28, which was IF positive, dose dependently inhibited the L-AP4 activity with an IC_{50} of 1.6 $nmol \cdot L^{-1}$ (Figure 2B). A total of five MABs that were shown to be positive in the IF assay were also found to be functional in the cAMP assay and dose-dependently inhibited $mGlu_7$ activities with low $nmol \cdot L^{-1}$ potencies (Figure 2D). These MABs are clearly $mGlu_7$ receptor specific, because they were not active in non-transfected CHO cells (Figure 2C).

MAB1/28, the most potent of the five MABs, was chosen for further investigation. Western blot from $rmGlu_7$-transfected cells under non-reducing conditions revealed that MAB1/28 recognized a high MW band around 188 kDa (Figure 3A), suggesting that it bound to $mGlu_7$ dimers, comparable to the Western blot using a rabbit polyclonal antibody (Figure 3B). Under reducing conditions where $rmGlu_7$ dimers are split into monomers, MAB1/28 could not recognize $mGlu_7$ receptors, suggesting a conformation-sensitive binding to $mGlu_7$ receptors (Figure 3A). However, bands with a MW around 188 kDa ($mGlu_7$ dimers) and 98 kDa ($mGlu_7$ monomer) were observed with rabbit polyclonal antibody raised against a peptide (C-NSPAAKKKYVSYNN) corresponding to amino acids 899–912 of human $mGlu_{7a}$ (Figure 3B). Therefore, monomer formation under reducing conditions could only be demonstrated by polyclonal antibody using $mGlu_7$-containing membranes (Figure 3B).

Mapping the epitope for the binding of MAB1/28 on the $mGlu_7$ receptor

To locate the binding site of the MAB1/28, the $rmGlu_6$ (871 aa), a closely related receptor with 80% aa similarity (65% aa identity) to that of $rmGlu_{7a}$ (915 aa), was used to generate $mGlu_6/mGlu_{7a}$ chimeras by exchanging their extracellular N-terminal domains (N-terminus: aa 1–565 of $rmGlu_6$ and aa 1–576 of $rmGlu_7$). Figure 4 shows immunostaining of intact cells expressing wild-type or chimeric $mGlu_6$ or $mGlu_7$ receptor, as indicated. Cells were stained after fixation and permeabilization with MAB1/28, then by secondary antibody labelled with Alexa Fluor 647. Only receptors with the

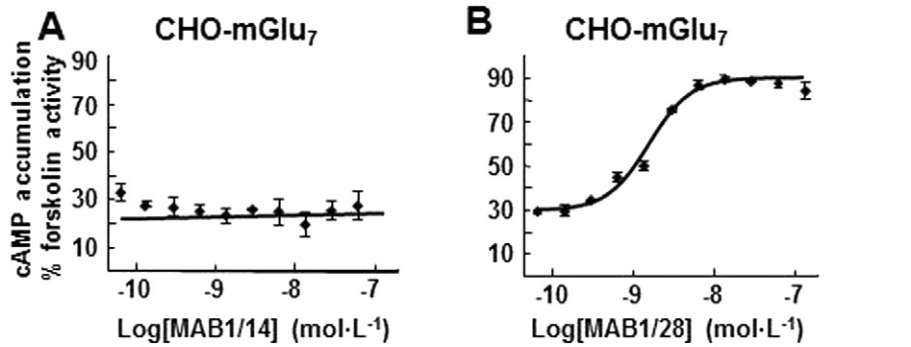

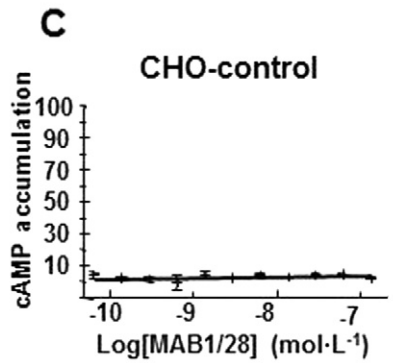

D

MAB#	cAMP assay IC_{50} (nmol·L^{-1})	efficacy (%)
1/6	inactive	
1/13	inactive	
1/14	inactive	
1/28	1.51 ± 0.08	100 ± 1
1/29	4.06 ± 1.22	97 ± 3
1/47	3.38 ± 0.22	92 ± 3
1/48	3.97 ± 0.95	104 ± 1
1/50	2.44 ± 0.20	94 ± 2

Figure 2

Pharmacological characterization of MABs in the cAMP assay. Concentration–response curve (CRC) of the MAB1/14 (A) and MAB1/28 (B) in the CHO rmGlu$_7$ expressing stable line and of the MAB1/28 in the non-transfected CHO control cells (C). Cells were stimulated with 3 μmol·L^{-1} forskolin, an EC_{80} of L-AP4 and various concentrations of IgG MABs. The cellular content of cAMP was measured and expressed as % cAMP content compared to cells treated with 3 μmol·L^{-1} forskolin only. (D) The IC_{50} and efficacy values for various MABs were calculated from CRCs as described in the Methods. All measurements were performed in duplicate and values represent the mean ± SD.

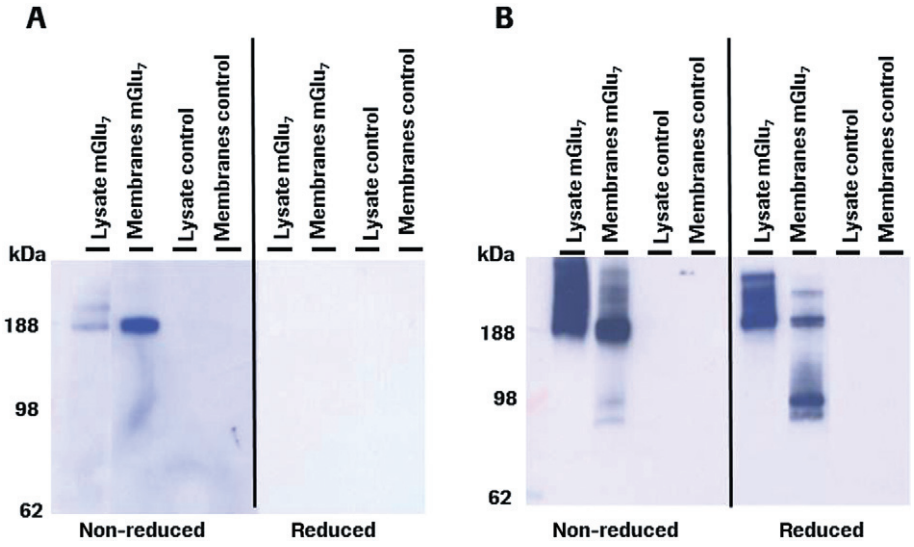

Figure 3

Western blot analysis. Samples containing cell lysate or membrane preparation from the CHO rmGlu$_7$ expressing stable line 83 or non-transfected CHO control cells under non-reduced or reduced conditions were loaded on 4–12% Nupage gel. (A) Blot incubated with anti-mGlu$_7$ MAB1/28 (mouse monoclonal IgG). (B) Blot incubated with anti-mGlu$_7$ rabbit polyclonal IgG from Upstate. A POD-labelled goat anti-mouse or anti-rabbit IgG antibody was used as a secondary antibody. The exposure times were 1 min and 5 s for mouse MAB1/28 and rabbit polyclonal antibodies respectively.

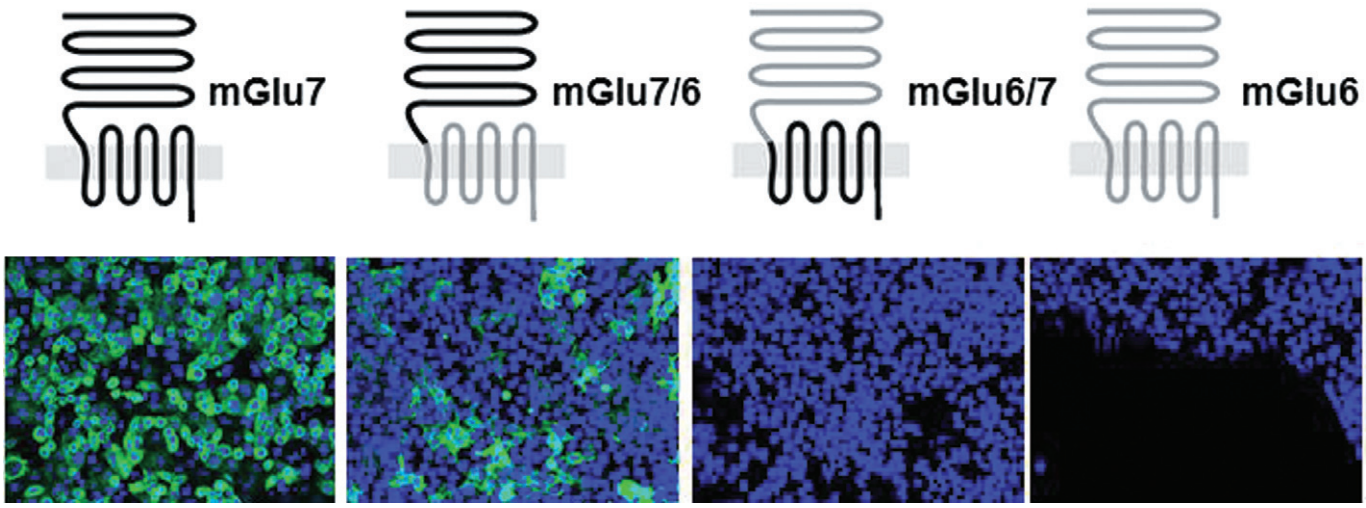

Figure 4

Immunofluorescence on cells expressing wild-type or chimeric rmGlu$_6$ or rmGlu$_7$ constructs. Cells were stained after fixation and permeabilization with MAB1/28-IgG followed by secondary antibody labelled with Alexa Fluor 647. In the top panel the predicted receptor topology is indicated relative to the membrane with the large extracellular domain at the top, with the mGlu$_6$ part in grey and mGlu$_7$ in black. Shown are representative overlaid images of immunostain (green) and nuclear stain (blue) acquired at 20 × magnification using same exposure parameters for the different are shown.

N-terminal domain of mGlu$_7$ receptors were recognized by MAB1/28 (Figure 4). This suggests that MAB1/28 binds within the N-terminus.

Immunohistochemistry in rodent brain sections

MAB1/28 was tested for binding to rat (Figure 5A) and mouse (Figure 5B, hippocampus shown enlarged) brain sections. Immunofluorescent staining was observed only when sections were mildly fixed with acetone rather than paraformaldehyde; this is probably due to the conformation-sensitive binding mode of MAB1/28. Most prominent immunoreactivity was found in regions in the hippocampal formation: hilus of dentate gyrus, stratum oriens and stratum radiatum of CA1 (Figure 5B). The selectivity of MAB1/28 for mGlu$_7$ receptor was further confirmed by immunofluorescent staining on the brain sections from age-matched mGlu$_7^{-/-}$ KO and mGlu$_7^{+/+}$ wild-type littermate mice. A strong immunoreactivity was only present in the brain region of wild-type mice (Figure 5C, hippocampus shown enlarged), while a lack of staining was observed in the brain sections of mGlu$_7^{-/-}$ KO mice (Figure 5D).

MAB1/28-induced internalization of receptor in mGlu$_7$ expressing CHO cells

When intact cells expressing rmGlu$_7$ were treated with directly fluorescein-labelled MAB1/28, both membrane-bound and internalized receptors were observed (Figure 6A), the latter appearing in a time-dependent manner (Supporting Information Figure S2). Receptor internalization was therefore triggered by MAB1/28 alone. The process was actively driven by the IgG and did not require co-stimulation by an agonist. Monovalently binding FAB fragments were generated by cleaving MAB1/28-IgG using papain (Figure 6E). The FAB fragments (Fab1) were used to investigate the effect of IgG versus Fab1 on internalization. HCS was used to quantify the internalization of receptor MAB1/28 complex by first staining the complex on the outside of the plasma membrane with one fluorophore and then, after permeabilization, staining the internalized complex with a different fluorescent dye. Figure 6B, F and J shows the homogenous intact cell staining with TrueBlue and the number, position and shape of the nuclei determined from the brighter Hoechst 33258 staining. Intact IgG (MAB1/28) and Fab1 fragments behave differently when incubated with mGlu$_7$ expressing CHO cells at 37°C. MAB1/28 is largely internalized (Figure 6C and D), while the Fab1 fragments are almost exclusively localized at the cell surface (Figure 6G and H). Surface staining and cytoplasmic spot intensity were highly specific to the MAB1/28, because no staining was observed when no MAB1/28 IgG or Fab1 was added excluded (Figure 6K and L). In addition, there was also no staining in non-transfected CHO-DUKX-CRE-luci control cells (Figure 6I). Surface staining and cytoplasmic spot intensity for MAB1/28- and Fab1-induced mGlu$_7$ internalization were quantified and results are shown (Figure 6M and N).

HCS was used to quantify the dose-dependency of the MAB1/28 or Fab1-induced internalization process. MAB1/28 and Fab1 fragments dose-dependently stained the plasma membrane (Figure 7B) and, as shown above, MAB1/28 was clearly dose-dependently internalized while the Fab1 fragments were only internalized to a very limited extent (Figure 7C). The pEC$_{50}$ values of 8.95 ± 0.15 (±SEM, n = 3) (EC$_{50}$ = 1.12 nmol·L^{-1}) for MAB1/28 membrane binding, 8.37 ± 0.42 (±SD, n = 2) (EC$_{50}$ = 4.27 nmol·L^{-1}) for Fab1 membrane staining and 8.38 ± 0.15 (±SEM, n = 3) (EC$_{50}$ = 4.17 nmol·L^{-1}) for MAB1/28 cytoplasmic spot intensity were determined from the concentration-dependent non-linear regression analysis (Figure 7B and C).

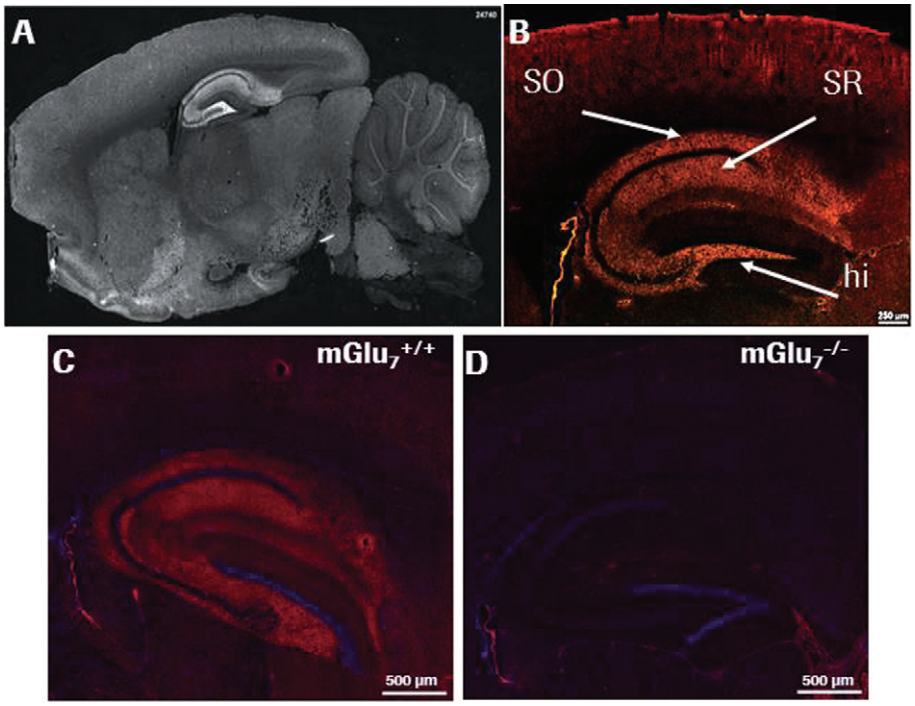

Figure 5

Staining of MAB1/28 in rodent brain sections. Indirect immunofluorescence staining with MAB1/28 revealed specific localization of mGlu$_7$ in the hippocampal formation as shown in an overview for rat brain (A) and in more detail for mouse brain with highest immunoreactive signals in stratum oriens (SO), stratum radiatum (SR) and hilus (hi) (B). Scale bars: 250 µm (white horizontal line in B). Immunoreactivity of MAB1/28 in the enlarged hippocampus of mGlu$_7^{+/+}$ wild-type mouse brain (C) and lack of MAB1/28 immunostaining in mGlu$_7^{-/-}$ knockout littermate mouse brain (D).

Kinetics of MAB1/28- and Fab1 fragment-induced mGlu$_7$ internalization and the effect of PTX

The kinetics of IgG-induced internalization were measured in mGlu$_7$ expressing CHO cells by image based analysis as described in Methods. The time course of surface membrane intensity for MAB1/28 showed that it declined continuously for 60 min while there was little change in the intensity of membrane fluorescence for Fab1 fragments (Figure 8A). The time course of internalization of MAB1/28 showed an increased accumulation in intracellular spot-like structures, with the curve rising for 60 min, but a very minor increase was detectable for the Fab1 fragments (Figure 8B). To determine the effect of PTX on MAB1/28- or Fab1-induced internalization, the experiment was carried out using the same protocol, with the modification that on the day of the experiment a solution of PTX in PBS (500 ng·mL^{-1}) was added to the wells 5 h before the incubation with the antibodies. As seen in Figure 8A and B, the PTX did not affect the MAB1/28- or Fab1-induced internalization of mGlu$_7$. This suggests that MAB1/28-induced receptor internalization does not depend on the cAMP signalling of the receptor.

Pharmacological characterization of MAB1/28 and Fab1 fragments in functional cAMP and GTPγ[^{35}S]-binding assays

Live CHO cells stably expressing rmGlu7 (line 83) and cAMP-Nano-TRF detection assay were used for functional characterization. Forskolin (3 µmol·L^{-1}) stimulated the AC activity to a 100% in these cells. The orthosteric (L-AP4) and selective allosteric (AMN082) agonists activated mGlu$_7$ receptors by dose-dependently inhibiting the forskolin-stimulated AC activity with EC$_{50}$ values of 44.3 and 0.256 µmol·L^{-1}, respectively (Figure 9A and B). In this context, as previously reported, L-AP4 had an EC$_{50}$ value of 175 µmol·L^{-1} at mGlu$_{7a}$ in the cAMP assay (Wu *et al.*, 1998) and AMN082 had EC$_{50}$ values of 64–290 nmol·L^{-1} as allosteric agonist at mGlu$_{7b}$, when measured in cAMP and [^{35}S]-GTPγ binding assays (Mitsukawa *et al.*, 2005). The activity of both agonists could be blocked using PTX (Figure 9A and B), indicating that, as expected, mGlu$_7$ signalling was mediated through the Gα$_i$ protein. The pharmacological activity of MAB1/28 and Fab1 fragments in the functional cAMP assay, along with its comparison to that of LY341495 (an orthosteric antagonist at mGlu$_2$, mGlu$_3$ and mGlu$_7$), is shown in Figure 9C and D. MAB1/28 dose-dependently antagonized both L-AP4 (EC$_{80}$ of 300 µmol·L^{-1}) and AMN082 (EC$_{80}$ of 1 µmol·L^{-1}) with similar IC$_{50}$ values of 2.4 nmol·L^{-1} (pIC$_{50}$ = 8.62) and 3.2 nmol·L^{-1} (pIC$_{50}$ = 8.49) respectively (Figure 9C and D). The Fab1 fragments partially antagonized both L-AP4 and AMN082 activities. Yet, again this hinted towards the requirement for bivalent binding of MAB1/28 in order to potently antagonize L-AP4 and AMN082 activities. As expected, pre-incubation with the orthosteric antagonist, LY341495, only antagonized the orthosteric agonist L-AP4, with an IC$_{50}$ of 486 nmol·L^{-1}, but not the allosteric agonist, AMN082 (Figure 9C and D). The IC$_{50}$ was in good agreement with that obtained in a radioligand binding

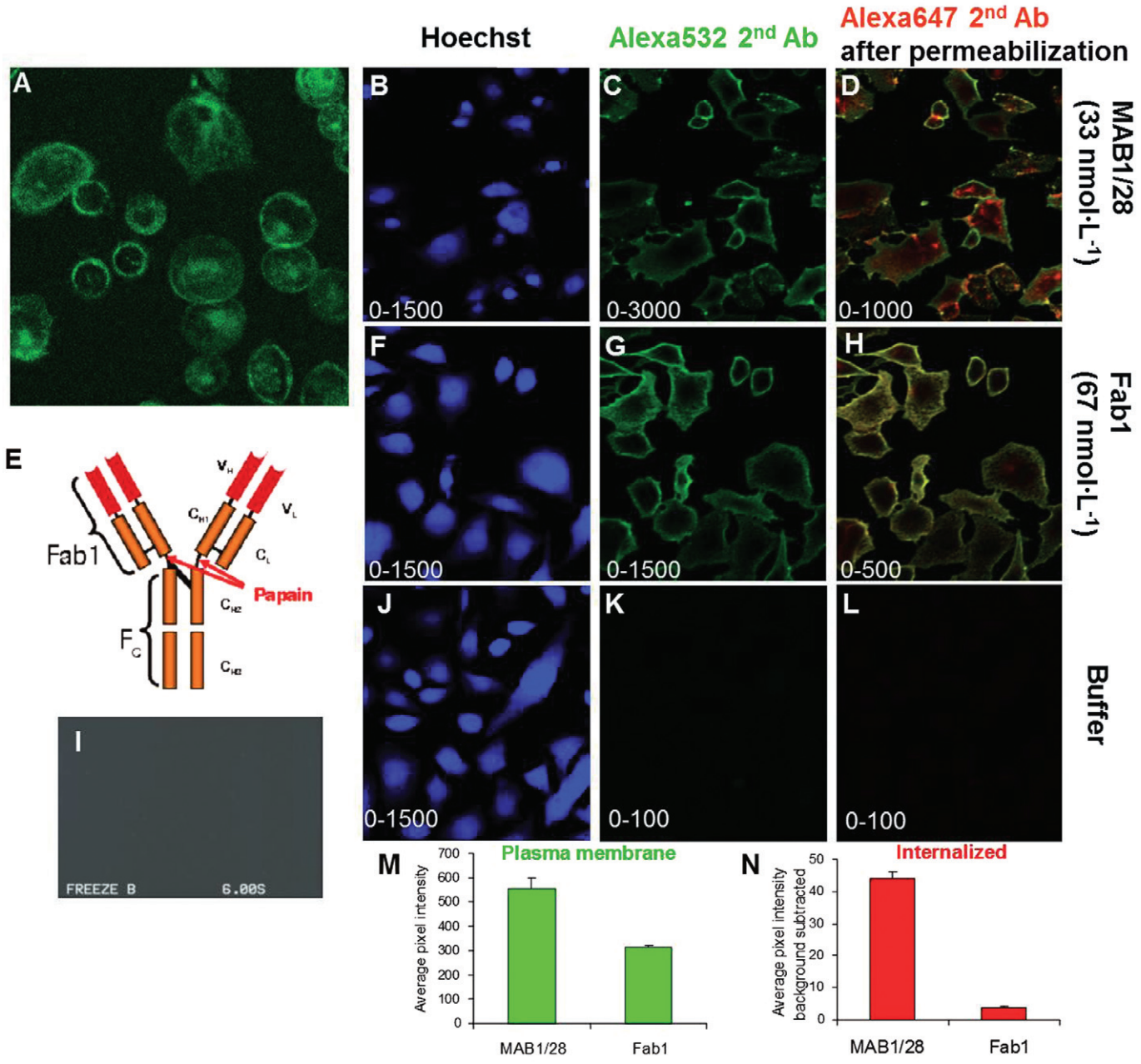

Figure 6

Comparison of MAB1/28 and Fab1 fragments induced $mGlu_7$ internalization. Direct immunofluorescence on live CHO-DUKX-CRE-luci-$rmGlu_{7a}$ stable cell line 83 (A) and non-transfected CHO-DUKX-CRE-luci control cells (I) by MAB1/28-Alexa488. E, tertiary protein structure of 1/28 type of antibody. Indicated is the papain enzyme cleavage site used for generation of monovalent Fab1 fragments. Images of CHO $mGlu_7$ expressing cells which have been incubated with 33 $nmol \cdot L^{-1}$ MAB1/28 as primary antibody (B–D), 67 $nmol \cdot L^{-1}$ Fab1 fragments (F–H) or with no primary antibody or Fab1 fragments (J–K) at 37°C before being washed and transferred to ice for secondary staining and fixation as described in the protocol. Each row contains images acquired in parallel of the same field of view in the well. (B, F and J) Images acquired with filter settings selective for TrueBlue and Hoechst 33258 stain (laser 405 nm, emission reflected by long path 650 filter, filtered through short path 568 filter and band path 455/70 filter). (C, G and K) Images acquired with filter settings selective for the cell surface stain with Alexa532 secondary antibody (laser 532 nm, emission reflected by LP650 and filtered through LP568 and BP586/40). (D, H and L) Images acquired with filter settings selective for the whole cell stain with Alexa647 secondary antibody after membrane permeabilization (laser 635 nm, emission passing through LP650 and filtered through BP690/50). The range of the pixel intensity grey scale ranging from black to white is indicated in lower left corner of the individual images. (M, N) The quantified surface staining and cytoplasmic spot intensity for, respectively, MAB1/28 and Fab1 fragments. Average pixel intensity in cell surface stain (M) and pixel intensity in cytoplasmic spots per cytoplasmic area (N).

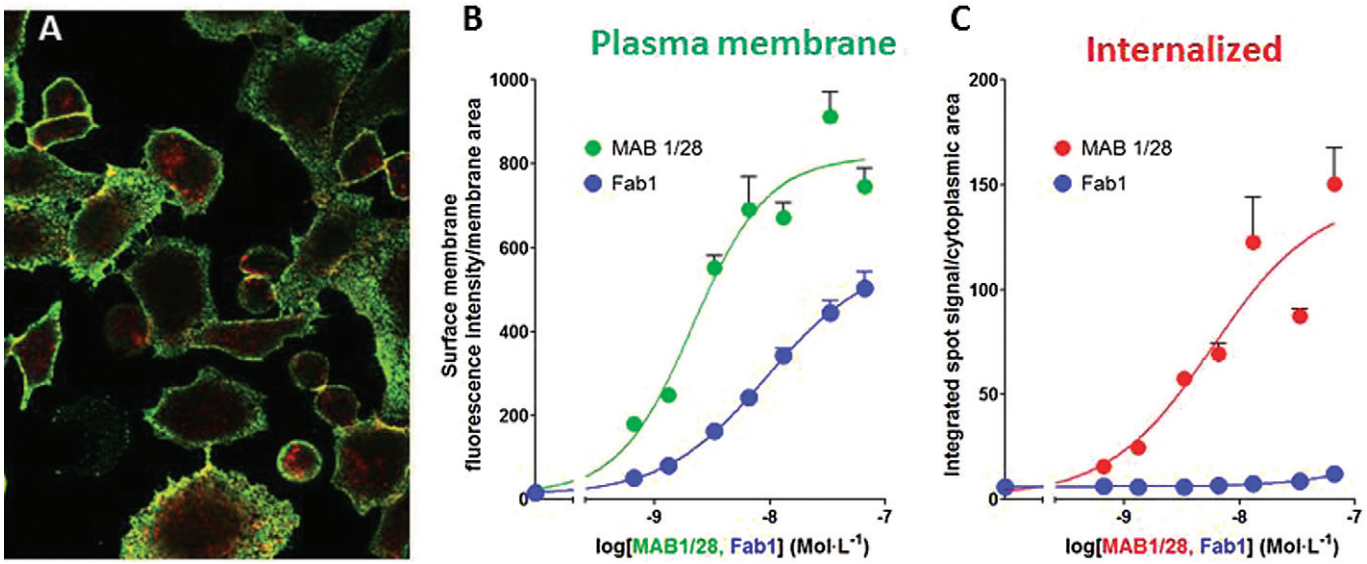

Figure 7

Image-based analysis of MAB1/28 internalization. (A) Cell surface (green; Alexa532, secondary antibody) and intracellular (red; Alexa647, secondary antibody after permeabilization) staining by MAB1/28 in the CHO mGlu$_7$ expressing cells. (B and C) Dose–response curves with different concentrations of MAB1/28 and Fab1 for plasma membrane staining and receptor-induced internalization. Average pixel intensity in cell surface stain (B) and pixel intensity in cytoplasmic spots per cytoplasmic area (C) are indicated. Each point is the average of three wells, shown as the mean ± SD. The graph is a representative of two independent experiments.

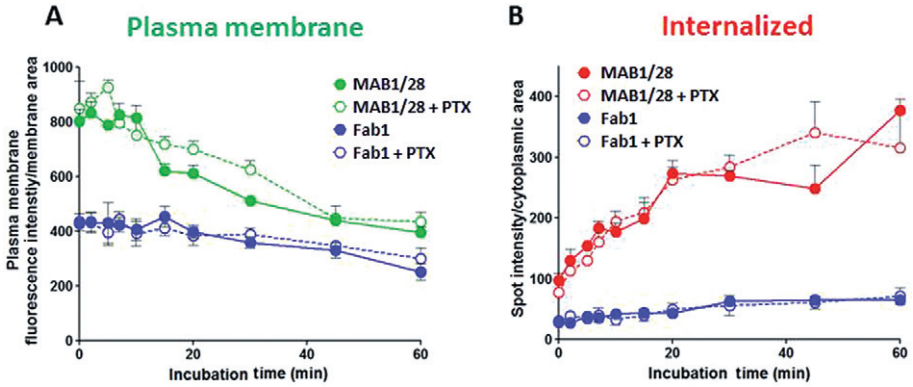

Figure 8

The kinetics of uptake of MAB1/28 and Fab1 fragments, and effect of pertussis toxin. Time course of pixel intensity in cell surface stain (A) and pixel intensity in cytoplasmic spots per cytoplasmic area (B) for MAB1/28 (22 nmol·L^{-1})- and Fab1 fragments (33 nmol·L^{-1})- induced receptor internalization in the stable CHO mGlu$_7$ expressing cells. The curve is representative of two independent experiments shown as mean ± SDM, each experiment carried out in triplicate. The effect of PTX pre-incubation on kinetic of MAB1/28 and Fab1 receptor-binding and internalization of mGlu$_7$ is also shown.

assay by Wright *et al*. (2000), where LY341495 exhibited a K_i value of 220 nmol·L^{-1} at mGlu$_{7a}$.

The L-AP4-induced stimulation of [^{35}S]-GTPγ binding in the membrane from CHO mGlu$_7$ expressing stable cells (line 83) was used to evaluate the pharmacology of MAB1/28 and its Fab1 fragments. Upon activation of the receptor by the agonist, the Gα protein releases GDP and dissociates from the receptor. The free site can be replaced by a non-hydrolysable [^{35}S]-GTPγ which can be measured in a binding assay. Only membranes from mGlu$_7$ expressing CHO cells were used in this assay, while live cells were used for the cAMP assay. Hence, one can investigate if the receptor blockade by MAB1/28 is mediated through the clearance of the receptor from the cell surface or through an arrest of the receptor conformation into an inactive state. L-AP4 (0.003–3 mmol·L^{-1}) elicited a concentration-dependent increase in the stimulation of [^{35}S]-GTPγ binding in the CHO mGlu$_7$ membranes with EC_{50}, Hill slope and E_{max} values of 129 μmol·L^{-1}, 1.8 and 148% respectively (Figure 9E). As seen in Figure 9E, the presence of 3 nmol·L^{-1} MAB1/28 caused a decrease in the E_{max} of the L-AP4

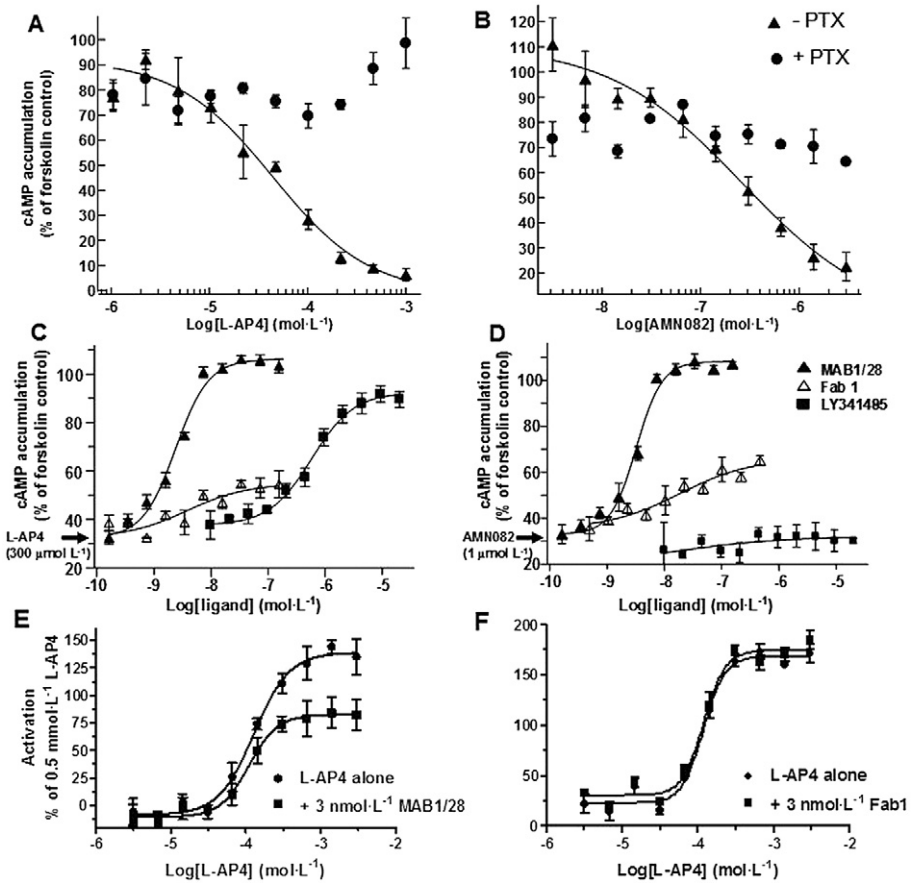

Figure 9

Functional characterization of MAB1/28 and Fab1 fragments in cAMP and [^{35}S]-GTPγ binding assays. Concentration–response curve of L-AP4 (A) and AMN082 (B) in the absence and presence of PTX in the CHO mGlu$_7$ expressing stable cell line 83. Cells were stimulated with 3 µmol·L^{-1} forskolin, and various concentrations of L-AP4 or AMN082. Concentration–dependent inhibition of 300 µmol·L^{-1} L-AP4 (C) and 1 µmol·L^{-1} AMN082 (D) by MAB1/28, Fab1 fragments or LY341495 in the CHO line 83 cells. Cells were stimulated with 3 µmol·L^{-1} forskolin, an EC$_{80}$ of L-AP4 or AMN082 and various concentrations of MAB1/28, Fab1 or LY341495. The cellular content of cAMP was measured and expressed as % cAMP content compared to cells treated with 3 µmol·L^{-1} forskolin only. Concentration–response curves for L-AP4-induced [^{35}S]-GTPγ binding in the membranes from CHO mGlu$_7$ cell line 83, in the absence and in the presence of 3 nmol·L^{-1} MAB1/28 (E) and in the absence and in the presence of 3 nmol·L^{-1} Fab1 fragments (F). All measurements were performed in triplicate and values represent mean ± SEM.

(93%) with a minor effect on EC$_{50}$ (110 µmol·L^{-1}) and Hill slope (2.2). The unchanged EC$_{50}$ suggests that MAB1/28 does not arrest the receptor conformation into an inactive state. The decrease in L-AP4 E$_{max}$ is in agreement with the mechanism that the blockade is mediated through the clearance of the receptor from the cell membrane. The Fab1 fragments had no effect on the L-AP4 concentration–response curve (Figure 9F), confirming that bivalent binding is required.

We also investigated whether the MAB1/28 could induce intracellular calcium release by using a fluo2-based assay. MAB1/28 was not able to promote calcium signalling in CHO-Gα15 mGlu$_7$ expressing cells, whereas Uridine 5′-triphosphate induced a robust response characterized by an EC$_{50}$ value of 250 nmol·L^{-1} (data not shown). To evaluate the selectivity of MAB1/28 relative to other mGlu receptors, the potency of MAB1/28 was tested for potential agonist and antagonist activity using a functional Ca^{2+} mobilization assay in the HEK-293 cell lines stably expressing hmGlu$_{1a}$, hmGlu$_2$ (+Gα16), hmGlu$_5$ and hmGlu$_8$ (+Gα15) in parallel with reference agonists and antagonists. Except for slight agonistic activity at hmGlu$_8$, MAB1/28 displayed no activity against other mGlu receptors (see Supporting Information Table S1 and Figure S1). Fab1 fragments, however, were devoid of any activity at hmGlu$_8$ (Supporting Information Figure S1G and H).

Involvement of MAPK/ERK signalling pathway in MAB1/28-induced receptor internalization

p44 and p42 MAPKs (also called ERK1 and ERK2), two similar (85% sequence identity) protein kinases, are among the widely expressed protein kinases of intracellular signalling molecules. They are activated through phosphorylation of threonine and tyrosine (Thr^{202} and Tyr^{204} of human MAPK or Thr^{183} and Tyr^{185} of rat MAPK) at the sequence T*EY* by a single upstream cell surface tyrosine kinase. To determine the intracellular signalling cascade involved in the MAB1/28-induced mGlu$_7$ receptor internalization, the phosphorylation

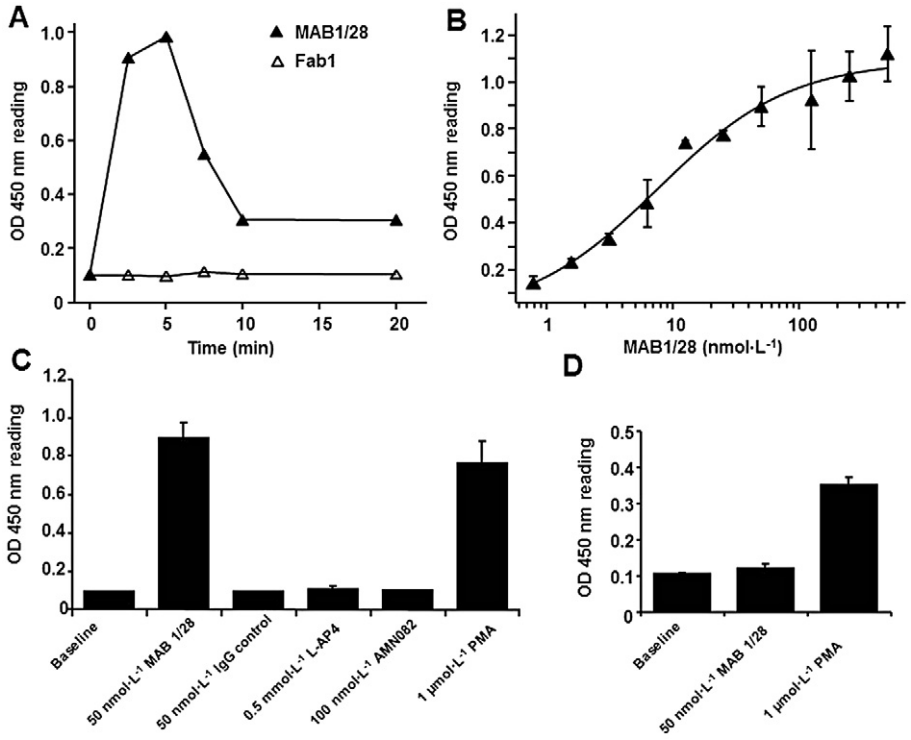

Figure 10

MAB1/28-mediated p44/42 MAPK (ERK1/2) phosphorylation. (A) A typical example of time course of p44/42 MAPK activation induced upon treatment with the 50 nmol·L^{-1} MAB1/28 in the CHO mGlu$_7$ expressing stable cell line 83. The phospho-p44/42 MAPK levels were determined by means of the PathScan Phospho-p44/42 MAPK Sandwich ELISA kit according to instructions of the manufacturer. Fab1 fragments had no effect on phospho-p44/42 MAPK level. (B) Increasing doses of MAB1/28 induced saturable levels of phospho-p44/42 MAPK 5 min after treatment of CHO cells expressing mGlu$_7$ receptors. (C) The specificity of the MAB1/28-induced levels of phospho-p44/42 MAPK after treatment of CHO cells expressing mGlu$_7$ receptors. (D) The effect on the levels of phospho-p44/42 MAPK of treatment with the MAB1/28 in the non-transfected CHO cells. The values represent the mean ± SEM from three measurements, each performed in triplicate.

of ERK1/2 was investigated in the CHO mGlu$_7$ stable line 83 using the PathScan® Phospho-p44/42 MAPK Sandwich ELISA kit. As revealed in the time course experiment (Figure 10A), the level of ERK1/2 phosphorylation transiently increased upon treatment with the MAB1/28 only, a maximum at roughly 5 min and rapidly declined thereafter. The maximal level of ERK1/2 phosphorylation exactly coincided with the time when the mGlu$_7$ receptors started to internalize as shown in Figure 8B. Furthermore, MAB1/28 triggered ERK1/2 phosphorylation in a dose-dependent manner with an EC_{50} of 7.5 nmol·L^{-1} (pEC_{50} = 8.12) (Figure 10B); hence, the potency of the MAB1/28 in triggering p44/42 MAPK activities is in the same order of magnitude as its potency in inhibiting the L-AP4-induced inhibition of forskolin activities (pIC_{50} of 8.62) as shown in Figure 9C or pEC_{50} of 8.95 from the receptor internalization assay (Figure 7B and C). However, a Fab1-mediated response could not be detected (Figure 10A).

As shown in Figure 10C, the efficacy of MAB1/28 on p44/42 MAPK activity was comparable to the levels obtained with the positive control PMA. In contrast to MAB1/28, an anti-6xHis IgG used as a control did not trigger an increase in p44/42 MAPK activities (Figure 10C). Of note is the absence of p44/42 MAPK activity after treatment of non-transfected CHO cells with the MAB1/28 in comparison to the activity obtained with the positive control PMA (Figure 10D), indicating that MAB1/28-mediated ERK1/2 phosphorylation is highly mGlu$_7$ specific. Moreover, the activity of the MAB1/28 cannot be triggered by the orthosteric mGlu$_7$ agonist L-AP4 or the allosteric mGlu$_7$ agonist AMN082 (Figure 10C). This suggests that MAB1/28 is a biased receptor agonist. Of note, it was shown in a recent study that the activation of mGlu$_7$ by L-AP4 resulted in stimulation of ERK1/2 in a HEK293 expression system (Wilkinson and Henley, 2011). We do not know the cause of the discrepancy between this report and our result; but we speculate that it might be due to differences in heterologous expression systems with different intracellular signalling pathways.

Discussion

Among mGlu receptors, the mGlu$_7$ receptors are of particular interest because they are strategically located at the site of vesicle fusion where they modulate the release of both the main excitatory and inhibitory neurotransmitters (Ferraguti and Shigemoto, 2006). They might, therefore, be the key regulator of synaptic transmission and plasticity. Thus, mGlu$_7$ could represent a potential therapeutic target for the treatment of a variety of neurological and psychiatric disorders. Due to the paucity of suitable selective ligands, our knowl-

edge of the precise role played by $mGlu_7$ in physiological and pathophysiological processes in the CNS is limited. In the current work, we describe the characterization of MAB1/28, an MAB raised against the extracellular, N-terminal domain of $mGlu_7$.

MAB1/28 is a selective, potent and functional anti-$mGlu_7$ MAB belonging to the IgG2a class. Its conformation-sensitive binding requires $mGlu_7$ in its native environment. High specificity of MAB1/28 for $mGlu_7$ was shown by the lack of IF staining in cells expressing $mGlu_1$, $mGlu_2$, $mGlu_3$, $mGlu_4$, $mGlu_5$, $mGlu_6$ or $mGlu_8$ receptor. IF staining with MAB1/28 in the rodent brain demonstrated an intense immunoreactivity in the hippocampal formation, which correlates well with previously published results using polyclonal antibodies (Shigemoto *et al.*, 1997; Kinoshita *et al.*, 1998; Sansig *et al.*, 2001). In addition, the high selectivity of MAB1/28 for $mGlu_7$ is confirmed by the absence of immunostaining in the $mGlu_7^{-/-}$ mice. We focused our analysis on the hippocampal formation, where, with the exception of $mGlu_4$ and $mGlu_6$, all other mGlu receptors are highly expressed (Shigemoto *et al.*, 1997). In a cAMP-functional assay, MAB1/28 potently antagonized both orthosteric (L-AP4) and allosteric (AMN082) $mGlu_7$ agonists with pIC_{50} of 8.62. Furthermore, the [^{35}S]-GTPγ functional assay showed that MAB1/28 decreased the maximal activation of the orthosteric agonist L-AP4 without a change in the EC_{50}. This antagonism of agonist responses by MAB1/28 is likely to act via $mGlu_7$ depletion from plasma membrane. Importantly, MAB1/28 actively triggered receptor internalization of $mGlu_7$ with a pEC_{50} (cell surface binding) of 8.95. This IgG (MAB1/28)-mediated endocytosis has several characteristics: (i) internalization occurs via a PTX-insensitive pathway and does not require $G\alpha_i$ protein activation; (ii) because monovalent Fab1 fragments of MAB1/28 lack effect, internalization requires divalent IgGs that interact with $mGlu_7$ receptor dimer; and (3) MAB1/28-induced internalization triggers the activation of the MAPK signalling pathway with a pEC_{50} of 8.12. Taken together, these data indicate that IgG-mediated internalization of $mGlu_7$ is different from classical agonist-mediated GPCR internalization, which requires the activation of G protein and involves the arrestin-, dynamin- and clathrin-dependent pathway (Lefkowitz, 1998). The same clathrin dependent mechanism is also underlying most agonist induced internalization of mGlu receptors (Dhami and Ferguson, 2006). Internalization of $mGlu_5$ and $mGlu_7$ has been described previously to be via a clathrin- and agonist-independent pathway in heterologous cells and in hippocampal neurons transiently transfected with N-terminally c-myc-tagged $mGlu_5$ (Fourgeaud *et al.*, 2003) and $mGlu_7$ (Lavezzari and Roche, 2007). In their report, Lavezzari and Roche observed the sucrose-insensitive nature of $mGlu_7$ receptor endocytosis, which suggested that the internalization process is independent of clathrin. The internalized $mGlu_7$ accumulated in ADP-ribosylation factor 6 (ARF6)-positive recycling endosomes, similar to other well-characterized proteins such as major histocompatibility complex class I and the glycosylphosphatidylinositol-anchored protein CD59. Furthermore, their data suggested that this mechanism applies to neurons. However, these authors did not consider IgG-mediated endocytosis, but assumed that anti-myc antibody binding to the N-terminally myc-tagged $mGlu_7$ is internalized as the result of a constitutive activity-driven mechanism. In this context, the antibody binding to an N-terminally epitope tagged receptor has previously been found to trigger the internalization of human muscarinic subtype 1 receptor (Tolbert and Lameh, 1998) and thyrotropin-releasing hormone receptor (Petrou *et al.*, 1997). In the current study, we speculate that the mechanism of $mGlu_7$ internalization is mainly driven by the antibody binding to the N-terminus of $mGlu_7$ receptors, but not by the receptor constitutive activity. In the above mentioned reports, a similar mechanism may also take place, suggesting that antibody binding to tagged receptors (myc-tag) can trigger internalization in recombinant cells as well as in neurons (Fourgeaud *et al.*, 2003; Lavezzari and Roche, 2007).

While MAB1/28 was unable to activate the receptor in a number of assays, it induced $mGlu_7$ internalization and triggered the activation of the MAPK/ERK pathway. In addition, the time of maximal level of ERK1/2 phosphorylation (5 min) coincided with the time when the $mGlu_7$ receptors started to be internalized. In contrast to MAB1/28, $mGlu_7$ orthosteric and allosteric agonists, L-AP4 and AMN082, did not activate the MAPK/ERK signalling pathway, demonstrating that G protein activation and receptor internalization can be completely dissociated. Indeed, numerous experimental data including the recent discovery of biased agonists (Rajagopal *et al.*, 2010) are consistent with the independence of G protein activation and receptor internalization. For example, morphine (μ-opioid receptor agonist) was unable to trigger endocytosis, whereas other ligands induced receptor internalization (Keith *et al.*, 1996). Similarly, a number of mutant receptors have been reported to be unable to signal, yet they internalize normally, whereas other mutants did not internalize in spite of their ability to signal normally (Hunyady *et al.*, 1994; Bennett *et al.*, 2000). In this regard, it has been suggested that GPCRs can adopt multiple active conformational states, each one corresponding to a specific, functionally distinct property (Thomas *et al.*, 2000; Blanpain *et al.*, 2002; Gupta *et al.*, 2007; Mancia *et al.*, 2007). Thus, different ligands can preferentially induce and/or stabilize one of these transient conformations. MAB1/28 stabilizes a conformation that triggers internalization. Moreover, the use of monovalent (Fab1) and bivalent (MAB1/28) forms allowed us to demonstrate that the internalization-prone conformation involves dimeric structures.

ARF6 (a member of the ARF family of Ras-related GTPases) was shown to be involved in the control of endocytic traffic in a variety of cell types (D'Souza-Schorey and Chavrier, 2006). ARF6 also regulates the internalization of ligands through a unique clathrin- and caveolae-independent pathway (Donaldson, 2003). Robertson *et al.* (2006) investigated the link between MAPK/ERK and ARF6 signalling pathways and showed that ERK signalling regulates trafficking through the clathrin-independent, ARF6 GTPase-regulated endosomal pathway. Moreover, this study has also indicated the importance of ERK signalling for the maintenance of normal morphology and dynamics of the ARF6 tubular endosome. However, the report by Tushir and D'Souza-Schorey (2007) showed that ARF6 and ERK activation states may well be codependent, as ARF6 activity can result in ERK activation. Interestingly, internalized $mGlu_7$ was shown to co-localize with ARF6-positive endosomes (Lavezzari and Roche, 2007),

which might be either recycled or subjected to lysosomal degradation. Although we did not investigate the involvement of β-arrestins in the MAB1/28 signalling pathway, accumulating evidence indicates that β-arrestins can also participate in G protein-independent intracellular signalling pathways via their interaction with signalling proteins like small-GTP-binding proteins and MAPK/ERK (Lefkowitz and Shenoy, 2005). Indeed, β-arrestin-mediated ARF6 activation has been shown to regulate β_2-adrenergic receptor endocytosis (Claing *et al.*, 2001). As shown for the angiotensin II, receptor type 1a (AT_{1a}) system, stimulation of the AT_{1a} receptor by a biased agonist, [SII] AngII (Ang II analogue) resulted in recruitment of β-arrestin2 and activation of ERK1/2 through Gαq/11-independent mechanism (Wei *et al.*, 2003; Aplin *et al.*, 2007). Similarly, a recent report has also demonstrated that a potent, selective β-arrestin-biased ligand of the AT_1 receptor, TRV120027, can selectively engage the β-arrestin-dependent MAPK pathway *in vitro* and *in vivo* (Violin *et al.*, 2010). From all these results, we propose a novel IgG-mediated receptor internalization pathway: MAB1/28 selectively binds to mGlu$_7$ receptor dimers (Fab1 fragments lack effect) and triggers a conformational change, which initiates the internalization process. mGlu$_7$ dimers internalize into ARF6-positive tubular recycling endosomes (Lavezzari and Roche, 2007) without activation of the G protein (PTX insensitive). Currently, we do not know at what level ERK1/2 is activated. Because inactivation of ERK has been shown to perturb recycling (Robertson *et al.*, 2006), we speculate that ARF6 may promote the activation of ERK at the tubular recycling endosomes.

The use of chimeric rmGlu$_7$/rmGlu$_6$ receptors allowed the mapping of the MAB1/28 binding to a large N-terminal domain (aa 1–576) of rmGlu$_7$. In this regard, a critical pocket adjacent to the glutamate binding site of mGlu receptors has recently been discovered (Selvam *et al.*, 2010; Acher *et al.*, 2011). Because the residues lining this pocket are highly divergent among mGlu receptors, it is plausible that MAB1/28 with its high selectivity might bind to this pocket. In summary, using an mGlu$_7$-specific monoclonal antibody, MAB1/28, we have identified a novel IgG-mediated GPCR internalization pathway involving the activation of MAPK/ERK signalling. We hypothesize that MAB1/28, acting as a biased agonist, induces and/or stabilizes a distinct and functionally specific receptor conformation, which can be internalized in the absence of G protein activation. To the best of our knowledge, MAB1/28 is the first MAB able to act as a biased agonist and promote endocytosis of a class C GPCR. Because MAB1/28 binds mGlu$_7$ with high affinity at a conformation-sensitive epitope, it can possibly stabilize the specific receptor conformation by increasing its hydrophilic surface and hence could be useful for mGlu$_7$ receptor crystallization. In addition, it may provide a potential screening tool for the discovery of new allosteric modulators of the mGlu$_7$ receptor. Of special interest is a recent report, which demonstrates that mGlu$_7$ signalling via an ERK-dependent mechanism regulates NMDA receptors. The activation of mGlu$_7$ resulted in the loss of surface NMDA receptor clusters and the depression of NMDA receptor currents in dissociated prefrontal cortex (PFC) pyramidal neurons (Gu *et al.*, 2012). One can assume that MAB1/28, with its high specificity for mGlu$_7$, should be an appropriate tool for investigating NMDA receptor trafficking and function in PFC neurons. It remains to be determined whether MAB1/28 could also exhibit *in vivo* activity. Thus, MAB1/28 as a biased agonist provides an invaluable biological tool for probing mGlu$_7$ function and selective activation of its intracellular trafficking.

Acknowledgements

We are grateful to Nadine Dahm, Krisztina Oroszlan-Szovik, Anja Osterwald, Bernard Rutten and Doris Zulauf for their excellent technical assistance, and Martin Benson for critical reading of the manuscript. mGlu7 knockout and wild-type littermate mice were generously made available by Herman Van der Putten, Novartis AG, Basel, Switzerland.

Conflict of interest

Authors (C. U., S. Z., B. B., H. M., L. L. and P. M.) are employees of F. Hoffmann-La Roche, Ltd.

References

Acher FC, Selvam C, Pin JP, Goudet C, Bertrand HO (2011). A critical pocket close to the glutamate binding site of mGlu receptors opens new possibilities for agonist design. Neuropharmacology 60: 102–107.

Airas JM, Betz H, El Far O (2001). PKC phosphorylation of a conserved serine residue in the C-terminus of group III metabotropic glutamate receptors inhibits calmodulin binding. FEBS Lett 494: 60–63.

Alexander SP, Mathie A, Peters JA (2011). Guide to receptors and channels (GRAC), 5th edn. Br J Pharmacol 164 (Suppl 1): S1–324.

Aplin M, Christensen GL, Schneider M, Heydorn A, Gammeltoft S, Kjolbye AL *et al.* (2007). Differential extracellular signal-regulated kinases 1 and 2 activation by the angiotensin type 1 receptor supports distinct phenotypes of cardiac myocytes. Basic Clin Pharmacol Toxicol 100: 296–301.

Bennett TA, Maestas DC, Prossnitz ER (2000). Arrestin binding to the G protein-coupled N-formyl peptide receptor is regulated by the conserved 'DRY' sequence. J Biol Chem 275: 24590–24594.

Blanpain C, Vanderwinden JM, Cihak J, Wittamer V, Le Poul E, Issafras H *et al.* (2002). Multiple active states and oligomerization of CCR5 revealed by functional properties of monoclonal antibodies. Mol Biol Cell 13: 723–737.

Cartmell J, Schoepp DD (2000). Regulation of neurotransmitter release by metabotropic glutamate receptors. J Neurochem 75: 889–907.

Claing A, Chen W, Miller WE, Vitale N, Moss J, Premont RT *et al.* (2001). Beta-arrestin-mediated ADP-ribosylation factor 6 activation and beta 2-adrenergic receptor endocytosis. J Biol Chem 276: 42509–42513.

Conn PJ, Pin JP (1997). Pharmacology and functions of metabotropic glutamate receptors. Annu Rev Pharmacol Toxicol 37: 205–237.

Cryan JF, Kelly PH, Neijt HC, Sansig G, Flor PJ, van Der Putten H (2003). Antidepressant and anxiolytic-like effects in mice lacking the group III metabotropic glutamate receptor mGluR7. Eur J Neurosci 17: 2409–2417.

D'Souza-Schorey C, Chavrier P (2006). ARF proteins: roles in membrane traffic and beyond. Nat Rev Mol Cell Biol 7: 347–358.

Dev KK, Nakajima Y, Kitano J, Braithwaite SP, Henley JM, Nakanishi S (2000). PICK1 interacts with and regulates PKC phosphorylation of mGLUR7. J Neurosci 20: 7252–7257.

DeWire SM, Ahn S, Lefkowitz RJ, Shenoy SK (2007). Beta-arrestins and cell signaling. Annu Rev Physiol 69: 483–510.

Dhami GK, Ferguson SS (2006). Regulation of metabotropic glutamate receptor signaling, desensitization and endocytosis. Pharmacol Ther 111: 260–271.

Donaldson JG (2003). Multiple roles for Arf6: sorting, structuring, and signaling at the plasma membrane. J Biol Chem 278: 41573–41576.

Drake MT, Violin JD, Whalen EJ, Wisler JW, Shenoy SK, Lefkowitz RJ (2008). Beta-arrestin-biased agonism at the beta2-adrenergic receptor. J Biol Chem 283: 5669–5676.

El Far O, Airas J, Wischmeyer E, Nehring RB, Karschin A, Betz H (2000). Interaction of the C-terminal tail region of the metabotropic glutamate receptor 7 with the protein kinase C substrate PICK1. Eur J Neurosci 12: 4215–4221.

El Far O, Bofill-Cardona E, Airas JM, O'Connor V, Boehm S, Freissmuth M *et al.* (2001). Mapping of calmodulin and Gbetagamma binding domains within the C-terminal region of the metabotropic glutamate receptor 7A. J Biol Chem 276: 30662–30669.

Fendt M, Schmid S, Thakker DR, Jacobson LH, Yamamoto R, Mitsukawa K *et al.* (2008). mGluR7 facilitates extinction of aversive memories and controls amygdala plasticity. Mol Psychiatry 13: 970–979.

Ferraguti F, Shigemoto R (2006). Metabotropic glutamate receptors. Cell Tissue Res 326: 483–504.

Foord SM, Bonner TI, Neubig RR, Rosser EM, Pin JP, Davenport AP *et al.* (2005). International Union of Pharmacology. XLVI. G protein-coupled receptor list. Pharmacol Rev 57: 279–288.

Fourgeaud L, Bessis AS, Rossignol F, Pin JP, Olivo-Marin JC, Hemar A (2003). The metabotropic glutamate receptor mGluR5 is endocytosed by a clathrin-independent pathway. J Biol Chem 278: 12222–12230.

Gesty-Palmer D, Chen M, Reiter E, Ahn S, Nelson CD, Wang S *et al.* (2006). Distinct beta-arrestin- and G protein-dependent pathways for parathyroid hormone receptor-stimulated ERK1/2 activation. J Biol Chem 281: 10856–10864.

Gu Z, Liu W, Wei J, Yan Z (2012). Regulation of NMDA receptors by metabotropic glutamate receptor 7. J Biol Chem 287: 10265–10275.

Gupta A, Decaillot FM, Gomes I, Tkalych O, Heimann AS, Ferro ES *et al.* (2007). Conformation state-sensitive antibodies to G-protein-coupled receptors. J Biol Chem 282: 5116–5124.

Hunyady L, Baukal AJ, Balla T, Catt KJ (1994). Independence of type I angiotensin II receptor endocytosis from G protein coupling and signal transduction. J Biol Chem 269: 24798–24804.

Keith DE, Murray SR, Zaki PA, Chu PC, Lissin DV, Kang L *et al.* (1996). Morphine activates opioid receptors without causing their rapid internalization. J Biol Chem 271: 19021–19024.

Kilkenny C, Browne W, Cuthill IC, Emerson M, Altman DG (2010). NC3Rs Reporting Guidelines Working Group. Br J Pharmacol 160: 1577–1579.

Kinoshita A, Shigemoto R, Ohishi H, van der Putten H, Mizuno N (1998). Immunohistochemical localization of metabotropic glutamate receptors, mGluR7a and mGluR7b, in the central nervous system of the adult rat and mouse: a light and electron microscopic study. J Comp Neurol 393: 332–352.

Kohler G, Milstein C (1975). Continuous cultures of fused cells secreting antibody of predefined specificity. Nature 256: 495–497.

Kosinski CM, Risso Bradley S, Conn PJ, Levey AI, Landwehrmeyer GB, Penney JB *et al.* (1999). Localization of metabotropic glutamate receptor 7 mRNA and mGluR7a protein in the rat basal ganglia. J Comp Neurol 415: 266–284.

Kunishima N, Shimada Y, Tsuji Y, Sato T, Yamamoto M, Kumasaka T *et al.* (2000). Structural basis of glutamate recognition by a dimeric metabotropic glutamate receptor. Nature 407: 971–977.

Lavezzari G, Roche KW (2007). Constitutive endocytosis of the metabotropic glutamate receptor mGluR7 is clathrin-independent. Neuropharmacology 52: 100–107.

Lefkowitz RJ (1998). G protein-coupled receptors. III. New roles for receptor kinases and beta-arrestins in receptor signaling and desensitization. J Biol Chem 273: 18677–18680.

Lefkowitz RJ, Shenoy SK (2005). Transduction of receptor signals by beta-arrestins. Science 308: 512–517.

Lindemann L, Jaeschke G, Michalon A, Vieira E, Honer M, Spooren W *et al.* (2011). CTEP: a novel, potent, long-acting, and orally bioavailable metabotropic glutamate receptor 5 inhibitor. J Pharmacol Exp Ther 339: 474–486.

McGrath J, Drummond G, Kilkenny C, Wainwright C(2010). Guidelines for reporting experiments involving animals: the ARRIVE guidelines. Br J Pharmacol 160: 1573–1576.

Mancia F, Brenner-Morton S, Siegel R, Assur Z, Sun Y, Schieren I *et al.* (2007). Production and characterization of monoclonal antibodies sensitive to conformation in the 5HT2c serotonin receptor. Proc Natl Acad Sci U S A 104: 4303–4308.

Masugi M, Yokoi M, Shigemoto R, Muguruma K, Watanabe Y, Sansig G *et al.* (1999). Metabotropic glutamate receptor subtype 7 ablation causes deficit in fear response and conditioned taste aversion. J Neurosci 19: 955–963.

Mitsukawa K, Yamamoto R, Ofner S, Nozulak J, Pescott O, Lukic S *et al.* (2005). A selective metabotropic glutamate receptor 7 agonist: activation of receptor signaling via an allosteric site modulates stress parameters *in vivo*. Proc Natl Acad Sci USA 102: 18712–18717.

Mitsukawa K, Mombereau C, Lotscher E, Uzunov DP, van der Putten H, Flor PJ *et al.* (2006). Metabotropic glutamate receptor subtype 7 ablation causes dysregulation of the HPA axis and increases hippocampal BDNF protein levels: implications for stress-related psychiatric disorders. Neuropsychopharmacology 31: 1112–1122.

Nakajima Y, Yamamoto T, Nakayama T, Nakanishi S (1999). A relationship between protein kinase C phosphorylation and calmodulin binding to the metabotropic glutamate receptor subtype 7. J Biol Chem 274: 27573–27577.

Niswender CM, Jones CK, Conn PJ (2005). New therapeutic frontiers for metabotropic glutamate receptors. Curr Top Med Chem 5: 847–857.

O'Connor V, El Far O, Bofill-Cardona E, Nanoff C, Freissmuth M, Karschin A *et al.* (1999). Calmodulin dependence of presynaptic metabotropic glutamate receptor signaling. Science 286: 1180–1184.

Palucha A, Klak K, Branski P, van der Putten H, Flor PJ, Pilc A (2007). Activation of the mGlu7 receptor elicits antidepressant-like effects in mice. Psychopharmacology (Berl) 194: 555–562.

Palucha-Poniewiera A, Branski P, Lenda T, Pilc A (2010). The antidepressant-like action of metabotropic glutamate 7 receptor agonist N,N'-bis(diphenylmethyl)-1,2-ethanediamine (AMN082) is serotonin-dependent. J Pharmacol Exp Ther 334: 1066–1074.

Perroy J, El Far O, Bertaso F, Pin JP, Betz H, Bockaert J *et al.* (2002). PICK1 is required for the control of synaptic transmission by the metabotropic glutamate receptor 7. EMBO J 21: 2990–2999.

Petrou C, Chen L, Tashjian AH Jr (1997). A receptor-G protein coupling-independent step in the internalization of the thyrotropin-releasing hormone receptor. J Biol Chem 272: 2326–2333.

Pin JP, Galvez T, Prezeau L (2003). Evolution, structure, and activation mechanism of family 3/C G-protein-coupled receptors. Pharmacol Ther 98: 325–354.

Pin JP, Kniazeff J, Goudet C, Bessis AS, Liu J, Galvez T *et al.* (2004). The activation mechanism of class-C G-protein coupled receptors. Biol Cell 96: 335–342.

Rajagopal S, Rajagopal K, Lefkowitz RJ (2010). Teaching old receptors new tricks: biasing seven-transmembrane receptors. Nat Rev Drug Discov 9: 373–386.

Robertson SE, Setty SR, Sitaram A, Marks MS, Lewis RE, Chou MM (2006). Extracellular signal-regulated kinase regulates clathrin-independent endosomal trafficking. Mol Biol Cell 17: 645–657.

Sansig G, Bushell TJ, Clarke VR, Rozov A, Burnashev N, Portet C *et al.* (2001). Increased seizure susceptibility in mice lacking metabotropic glutamate receptor 7. J Neurosci 21: 8734–8745.

Scheschonka A, Findlow S, Schemm R, El Far O, Caldwell JH, Crump MP *et al.* (2008). Structural determinants of calmodulin binding to the intracellular C-terminal domain of the metabotropic glutamate receptor 7A. J Biol Chem 283: 5577–5588.

Schoepp DD, Jane DE, Monn JA (1999). Pharmacological agents acting at subtypes of metabotropic glutamate receptors. Neuropharmacology 38: 1431–1476.

Selvam C, Oueslati N, Lemasson IA, Brabet I, Rigault D, Courtiol T *et al.* (2010). A virtual screening hit reveals new possibilities for developing group III metabotropic glutamate receptor agonists. J Med Chem 53: 2797–2813.

Shigemoto R, Kinoshita A, Wada E, Nomura S, Ohishi H, Takada M *et al.* (1997). Differential presynaptic localization of metabotropic glutamate receptor subtypes in the rat hippocampus. J Neurosci 17: 7503–7522.

Somogyi P, Dalezios Y, Lujan R, Roberts JD, Watanabe M, Shigemoto R (2003). High level of mGluR7 in the presynaptic active zones of select populations of GABAergic terminals innervating interneurons in the rat hippocampus. Eur J Neurosci 17: 2503–2520.

Sukoff Rizzo SJ, Leonard SK, Gilbert A, Dollings P, Smith DL, Zhang MY *et al.* (2011). The metabotropic glutamate receptor 7 allosteric modulator AMN082: a monoaminergic agent in disguise? J Pharmacol Exp Ther 338: 345–352.

Thomas WG, Qian H, Chang CS, Karnik S (2000). Agonist-induced phosphorylation of the angiotensin II (AT(1A)) receptor requires generation of a conformation that is distinct from the inositol phosphate-signaling state. J Biol Chem 275: 2893–2900.

Tian Y, Liu Y, Chen X, Kang Q, Zhang J, Shi Q *et al.* (2010). AMN082 promotes the proliferation and differentiation of neural progenitor cells with influence on phosphorylation of MAPK signaling pathways. Neurochem Int 57: 8–15.

Tolbert LM, Lameh J (1998). Antibody to epitope tag induces internalization of human muscarinic subtype 1 receptor. J Neurochem 70: 113–119.

Tushir JS, D'Souza-Schorey C (2007). ARF6-dependent activation of ERK and Rac1 modulates epithelial tubule development. EMBO J 26: 1806–1819.

Violin JD, DeWire SM, Yamashita D, Rominger DH, Nguyen L, Schiller K *et al.* (2010). Selectively engaging beta-arrestins at the angiotensin II type 1 receptor reduces blood pressure and increases cardiac performance. J Pharmacol Exp Ther 335: 572–579.

Wei H, Ahn S, Shenoy SK, Karnik SS, Hunyady L, Luttrell LM *et al.* (2003). Independent beta-arrestin 2 and G protein-mediated pathways for angiotensin II activation of extracellular signal-regulated kinases 1 and 2. Proc Natl Acad Sci USA 100: 10782–10787.

Wilkinson KA, Henley JM (2011). Analysis of metabotropic glutamate receptor 7 as a potential substrate for SUMOylation. Neurosci Lett 491: 181–186.

Wright RA, Arnold MB, Wheeler WJ, Ornstein PL, Schoepp DD (2000). Binding of [3H](2S,1'S,2'S)-2-(9-xanthylmethyl)-2-(2'-carboxycyclopropyl) glycine ([3H]LY341495) to cell membranes expressing recombinant human group III metabotropic glutamate receptor subtypes. Naunyn Schmiedebergs Arch Pharmacol 362: 546–554.

Wu S, Wright RA, Rockey PK, Burgett SG, Arnold JS, Rosteck PR *et al.* (1998). Group III human metabotropic glutamate receptors 4, 7 and 8: molecular cloning, functional expression, and comparison of pharmacological properties in RGT cells. Brain Res Mol Brain Res 53: 88–97.

Supporting Information

Additional Supporting Information may be found in the online version of this article:

Figure S1 Selectivity of MAB1/28 towards mGlu receptors. MAB1/28 displayed no effect as agonist or antagonist in the HEK-293 cell lines stably expressing hmGlu$_{1a}$ (A & B), hmGlu$_2$ (+Gα16) (C & D), hmGlu$_5$ (E & F) and hmGlu$_8$ (+Gα15) (G & H) using functional Ca^{2+} mobilization assay. The activity of reference agonists and antagonists is shown for comparison. At least three independent experiments were performed in duplicate. Error bars represent ± SEM.

Figure S2 Time-lapse sequence of internalizing mGlu7 receptors in intact cells. CHO cells expressing mGlu7 were incubated with directly fluorescein-labelled MAB1/28 on ice for 1 h and then returned to conditioned media for 6, 10, 18, 33 and 53 min to allow internalization. Confocal images suggest newly formed spot-like structures to be intracellular and forming in a time-dependent manner.

Table S1 Selectivity of MAB1/28 towards mGlu receptors. Potencies of MAB1/28 and MAB1/28-derived Fab1 fragments on human $mGlu_1$, $mGlu_2$, $mGlu_5$ and $mGlu_8$ measured in Ca^{2+} mobilization assays configured for the detection of agonism or antagonism of test compounds. The concentration for the antibody and Fab1 fragments refers to the protein concentration, not to the concentration of binding sites. The mean results of several experiments performed in duplicate (reference agonists/antagonists) or as single experiments (MAB1/28/Fab1) ± SDM are reported. (1*S*,2*S*,5*R*,6*S*)-2-aminobicyclo[3.1.0]hexane-2,6-dicarboxylic acid (LY354740): $mGlu_2/mGlu_3$ agonist. 7-(hydroxyimino) cyclopropan[b]chromen-1a-carboxylic acid ethyl ester (CPCCOEt): $mGlu_1$ NAM. 2-methyl-6-(phenylethyl)-pyridine (MPEP): $mGlu_5$ NAM. (*RS*)-α-methylserine-o-phosphate (MSOP): group III mGlu antagonist.